ANTIOXIDANTS & REDOX SIGNALING
Volume 27, Number 9, 2017

DOI: 10.1089/ars.2016.6831

Discoveries

ORIGINAL RESEARCH COMMUNICATION

Inhibition of NFE2L2-Antioxidant Response Element Pathway by Mitochondrial Reactive Oxygen Species Contributes to Development of Cardiomyopathy and Left Ventricular Dysfunction in Chagas Disease

Jake Jianjun Wen,[1] Craig Porter,[2,3] and Nisha Jain Garg[1,4,5]

Abstract

Aims: We investigated the effects of mitochondrial reactive oxygen species (mtROS) on nuclear factor (erythroid 2)-like 2 (NFE2L2) transcription factor activity during *Trypanosoma cruzi* (*Tc*) infection and determined whether enhancing the mtROS scavenging capacity preserved the heart function in Chagas disease.

Results: C57BL/6 wild type (WT, female) mice infected with *Tc* exhibited myocardial loss of mitochondrial membrane potential, complex II (CII)-driven coupled respiration, and ninefold increase in mtROS production. *In vitro* and *in vivo* studies showed that *Tc* infection resulted in an ROS-dependent decline in the expression, nuclear translocation, antioxidant response element (ARE) binding, and activity of NFE2L2, and 35–99% decline in antioxidants' (gamma-glutamyl cysteine synthase [γGCS], heme oxygenase-1 [HO1], glutamate-cysteine ligase modifier subunit [GCLM], thioredoxin (Trx), glutathione S transferase [GST], and NAD(P)H dehydrogenase, quinone 1 [NQO1]) expression. An increase in myocardial and mitochondrial oxidative adducts, myocardial interventricular septum thickness, and left ventricle (LV) mass, a decline in LV posterior wall thickness, and disproportionate synthesis of collagens (COLI/COLIII), αSMA, and SM22α were noted in WT.*Tc* mice. Overexpression of manganese superoxide dismutase (MnSOD) in cultured cells (HeLa or cardiomyocytes) and MnSOD^{tg} mice preserved the NFE2L2 transcriptional activity and antioxidant/oxidant balance, and cardiac oxidative and fibrotic pathology were significantly decreased in MnSOD^{tg}.*Tc* mice. Importantly, echocardiography finding of a decline in LV systolic (stroke volume, cardiac output, ejection fraction) and diastolic (early/late peak filling ratio, myocardial performance index) function in WT.*Tc* mice was abolished in MnSOD^{tg}.*Tc* mice.

Innovation and Conclusion: The mtROS inhibition of NFE2L2/ARE pathway constitutes a key mechanism in signaling the fibrotic gene expression and evolution of chronic cardiomyopathy. Preserving the NFE2L2 activity arrested the mitochondrial and cardiac oxidative stress, cardiac fibrosis, and heart failure in Chagas disease. *Antioxid. Redox Signal.* 27, 550–566.

Keywords: cardiac remodeling, Chagas disease, LV dysfunction, mitochondrial respiration, MnSOD, NFE2L2, *Trypanosoma cruzi*

Introduction

CHAGASIC CARDIOMYOPATHY (CCM) IS caused by the protozoan *Trypanosoma cruzi* (*Tc* or *T. cruzi*) and represents the third largest tropical disease burden globally (46). Infected individuals exhibit an acute phase of peak blood parasitemia that is resolved in 2–3 months. Approximately 30–40% of infected individuals progress to present a complex and diverse clinical outcome. The major complications of chronic infection by *T. cruzi* include

[1]Department of Microbiology and Immunology, University of Texas Medical Branch (UTMB), Galveston, Texas.
[2]Metabolism Unit, Shriners Hospital for Children, Galveston, Texas.
Departments of [3]Surgery and [4]Pathology, University of Texas Medical Branch (UTMB), Galveston, Texas.
[5]Institute for Human Infections and Immunity, University of Texas Medical Branch (UTMB), Galveston, Texas.

Innovation

Our results provide the first evidence that mitochondrial oxidative metabolic capacity is compromised, and mitochondrial reactive oxygen species inhibition of nuclear factor (erythroid 2)-like 2 (NFE2L2) transcriptional activity contributes to heart failure in chagasic cardiomyopathy (CCM). Parasite burden was not correlated to disease state, rather, host's inability to preserve NFE2L2 activity and halt mitochondrial and cardiac oxidative adducts constituted a key mechanism in signaling the fibrotic gene expression that eventually evolved as chronic cardiomyopathy. The detailed analysis of left ventricle systolic and diastolic performance in chagasic wild type and manganese superoxide dismutase^{tg} mice conclusively demonstrates that NFE2L2 is an important therapeutic target for maintaining the cardiac performance in heart failure of infectious (and other) etiologies.

ventricular fibrillation, thromboembolism, and congestive heart failure (45, 47).

The clinical outcomes of CCM are related to the virulence of the parasite strain as well as to the host response to infection. Histological evaluation of cardiac biopsies revealed diffused and patchy myocarditis, interstitial mononuclear cell infiltrates, and myocardial fiber destruction during progressive disease (25). Transcriptomic profiling of *Tc*-infected cardiomyocytes (50) suggested that activation of both TGF-β-dependent and TGF-β-independent fibrotic pathways could contribute to hypertrophy. Studies using a three-dimensional cardiomyocyte culture model showed that *Tc* infection increased the cellular and extracellular matrix components, mimicking fibrotic cardiac remodeling (21). Chemokine signaling and interferon gamma have also been implicated in the progression of cardiac fibrosis in chagasic patients (12). However, molecular mechanisms of cardiac fibrosis and how myocardial injuries are sustained during Chagas disease are not completely understood.

Studies in experimental models and humans have demonstrated that the infected host sustains oxidative stress because of increased mitochondrial reactive oxygen species (mtROS) production in the myocardium [reviewed in Gupta *et al.* (23), Zacks *et al.* (59)]. The pro-oxidant milieu was evidenced by peripheral and myocardial increase in protein carbonyls and lipid hydroperoxides in progressive CCM (56). Mitochondria normally utilize manganese superoxide dismutase (MnSOD) to dismutate the superoxide that can be further reduced by glutathione peroxidases and other antioxidants (11), and thus cellular metabolic homeostasis is maintained (48). However, MnSOD activity was decreased (56, 57), and glutathione antioxidant defense was nonresponsive to increased oxidative stress in chagasic rodents (56) and human patients (57). Why antioxidant response is not triggered in the presence of continued oxidative stress in chagasic myocardium is not known.

The transcription factor nuclear factor (erythroid 2)-like 2 (NFE2L2) (also called Nrf2) is an important component of the intracellular antioxidant machinery. NFE2L2 transactivates genes with antioxidant response elements (AREs), and it coordinates the expression of cytoprotective genes to counteract endogenously or exogenously generated oxidative stress (29).

In this study, we aimed to determine whether NFE2L2 transcriptional activity was compromised and contributed to nonresponsiveness of the antioxidant response during *Tc* infection. We also investigated whether mtROS affected the NFE2L2–ARE activity and whether enhancing the mtROS scavenging capacity preserved the NFE2L2-dependent antioxidant/oxidant balance and subsequently the heart function in Chagas disease. For this, we employed the *in vitro* transient transfection approach and genetically modified mice with increased mtROS scavenging capacity and performed all studies in comparison with sex, age, and genetically matched wild type (WT) controls. We utilized the fluorescence- and luminescence-based probes, biochemical and molecular assays, and cutting-edge *in situ* respirometry and three-dimensional echocardiography (ECG) to test our hypothesis.

Our results suggested that mtROS-induced decline in NFE2L2 activity is a key event in continuous presentation of antioxidant/oxidant imbalance, cardiac hypertrophy, and left ventricle (LV) systolic and diastolic dysfunction in chagasic myocardium. We discuss the benefits of MnSOD/mtROS balance in preserving the NFE2L2 transcriptional activity and cardiac structure and function in chronic heart disease.

Results

C57BL/6 female mice infected with 10,000 *Tc* exhibit parasite dissemination to tissues within 4 days postinfection (pi), peak parasitemia during 14–45 days pi, and develop chronic disease during 120–150 days pi (20). We employed this well-established model of infection to WT and MnSOD^{tg} mice in this study. WT and MnSOD^{tg} mice were genotyped by polymerase chain reaction (PCR) amplification of 230 and 587 bp fragments, respectively (Supplementary Fig. S1A; Supplementary Data are available online at www.liebertpub.com/ars). We evaluated the levels of MnSOD messenger RNA (mRNA), protein, and activity in WT and MnSOD^{tg} mice and the effect of *Tc* infection on MnSOD levels. The basal levels of MnSOD mRNA, protein, and enzymatic activity were 123%, 55%, and 50% higher in MnSOD^{tg} (*vs.* WT) mice (Supplementary Fig. S1B–D, all $^{\#}p<0.05$). Chronically infected WT mice exhibited 29%, 63.6%, and 80% decline in myocardial levels of MnSOD mRNA, protein, and activity, respectively, compared with that noted in WT controls (Supplementary Fig. S1B–D, all, $^{*}p<0.001$). In MnSOD^{tg} mice, *Tc* infection resulted in only a 10%, 13.4%, and 28% decline in the levels of MnSOD mRNA, protein, and enzymatic activity, respectively (Supplementary Fig. S1B–D). These results confirmed the genotype of the MnSOD^{tg} mice, and suggested that MnSOD expression and activity were significantly compromised in chagasic WT mice. Because of the enhanced basal level of MnSOD, chronically infected MnSOD^{tg} mice maintained the MnSOD levels above or similar to that noted in normal WT controls.

To determine whether MnSOD level influences the mitochondrial function, we monitored the oxidative phosphorylation (OXPHOS) capacity in freshly isolated heart tissue slices by using an Oxygraph-2k (O2K) system (Fig. 1). No significant differences in basal levels of mitochondrial respiration were observed in myocardial fibers of normal MnSOD^{tg} and WT mice. In response to chronic *Tc* infection, state 4

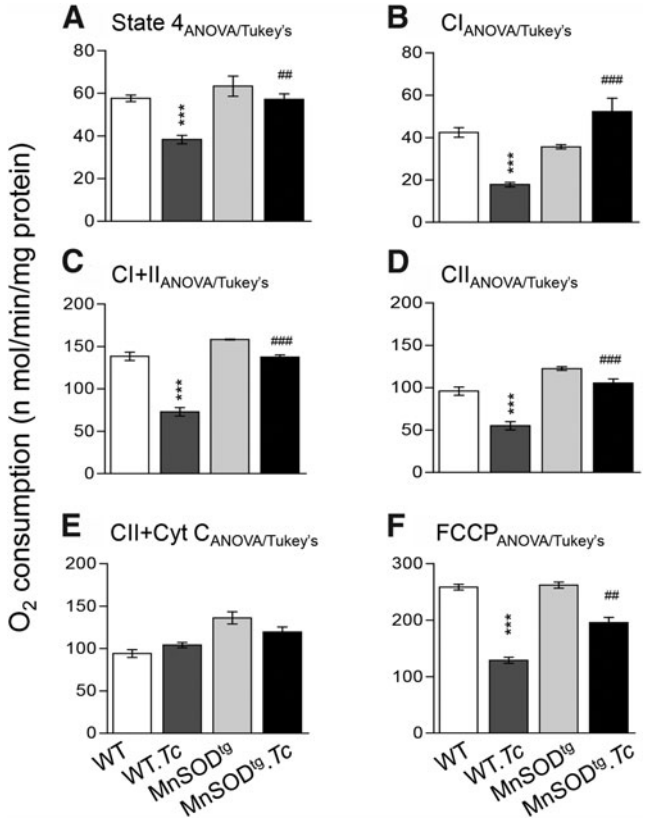

FIG. 1. ***In situ*** **mitochondrial respiration in heart tissue slices of chronically infected MnSOD^{tg} mice.** C57BL/6 female mice (WT and MnSOD^{tg}) were infected with *Trypanosoma cruzi* and harvested at 120 days pi. Cardiac myofiber bundles ($\sim$2 mg) were permeabilized, and mitochondrial respiratory function was measured using an Oxygraph-2k respirometer. Baseline respiration was recorded with myofiber bundles alone, and state 4 leak respiration **(A)** supported by electron flow through CI substrates (pyruvate+glutamate+ malate, P+G+M) was recorded. Then, ADP-coupled state 3 respiration with electron input from CI **(B)** was recorded. Next, succinate was added to record CI+CII-supported state 3 **(C)** and rotenone (inhibits CI) was added to record CII-supported state 3 **(D)** respiration. Competence of the outer mitochondrial membrane and maximal electron transfer capacity were assessed with addition of cytochrome c **(E)** and FCCP **(F)**, respectively. Data are plotted as mean value $\pm$ SEM ($n = 6$–10 mice per group), and significance is shown as **Tc*-infected *versus* matched control or $^{\#}$WT.*Tc* *versus* MnSOD^{tg}.*Tc*, and presented as $^{\#\#}p < 0.01$, $^{***,\#\#\#}p < 0.001$. The statistical tests employed for calculating the significance (Student's *t* test, ANOVA/Tukey's, Kruskal–Wallis with Dunn's test [K-W/Dunn's], and Mann–Whitney [M-W]) are shown with figure panels. ANOVA, analysis of variance; CI, complex I; CII, complex II; FCCP, carbonyl cyanide-4-(trifluoromethoxy)phenyl-hydrazone; MnSOD, manganese superoxide dismutase; pi, postinfection; SEM, standard error of the mean; *Tc* or *T. cruzi*, *Trypanosoma cruzi*; WT, wild type.

respiration driven by complex I (CI) substrates, and ADP-coupled state 3 respiration (indicates proton gradient for ATP synthesis) driven by electron input from CI, CI+complex II (CII), and CII substrates were decreased by 33.5%, 58%, 47%, and 42.7%, respectively, in the myocardial fibers of WT.*Tc* (*vs.* WT) mice (Fig. 1A–D, all, $^{*}p < 0.001$). The CII-driven respiration was normalized to control levels with addition of cytochrome c in the myocardial fibers of WT chagasic mice, thus suggesting that the integrity of mitochondrial outer membrane was affected by *Tc* infection (Fig. 1E). In comparison, myocardial fibers of MnSOD^{tg} mice exhibited no significant effect of *Tc* infection on the rate of CI-driven state 4 respiration, and CI-, CI+CII-, and CII-driven state 3 respirations, and no effect of cytochrome c addition on mitochondrial respiration (Fig. 1A–E). The mitochondrial respiration capacity in the presence of carbonyl cyanide-4-(trifluoromethoxy)phenyl-hydrazone (FCCP) ionophore that dissipates the chemiosmotic gradient leaving the electron transport system uninhibited was decreased by 50% ($^{*}p < 0.001$) and 22% in WT.*Tc* and MnSOD^{tg}.*Tc* (*vs.* matched controls) mice, respectively (Fig. 1F).

We confirmed the benefits of MnSOD in preserving OXPHOS capacity in chagasic heart by using the isolated cardiac mitochondria (Supplementary Fig. S2). As observed in myocardial fibers (Fig. 1), isolated cardiac mitochondria of WT and MnSOD^{tg} mice exhibited no significant difference in CI- and CII-driven respiration and ADP/O ratio that indicates ATP synthesis (Supplementary Fig. S2A–C). The CI-driven state 4 and state 3 respirations and ADP/O ratio were decreased by 63%, 51%, and 27%, respectively, in isolated cardiac mitochondria of WT.*Tc* (*vs.* WT, all, $^{*}p < 0.01$) mice, and by 54%, 27%, and 12%, respectively, in isolated cardiac mitochondria of MnSOD^{tg}.*Tc* (*vs.* MnSOD^{tg}) mice (Supplementary Fig. S2A.a–C.a). The CII-driven state 4 was not changed, whereas state 3 respiration and ADP/O ratio were decreased by 43.7% and 75%, respectively, in isolated cardiac mitochondria of WT.*Tc* (*vs.* WT, all, $^{*}p < 0.01$) mice, and by 19% and 26%, respectively, in MnSOD^{tg}.*Tc* (*vs.* MnSOD^{tg}) mice (Supplementary Fig. S2A.b–C.b). Respiratory control ratio (RCR, indicates mitochondrial integrity) was not disturbed in CI respiring mitochondria from any of the *Tc*-infected mice (Supplementary Fig. S2D.a), whereas CII-driven RCR was decreased by 62% and 17% in WT.*Tc* ($^{*}p < 0.01$) and MnSOD^{tg}.*Tc* mice in comparison with matched controls (Supplementary Fig. S2D.b). Together the results presented in Figure 1 and Supplementary Figure S2 suggested that mitochondrial chemiosmosis gradient (*i.e.*, CI-driven state 4) and CI- and CII-driven coupled respiration were significantly compromised in cardiac mitochondria of chagasic WT mice, and MnSOD overexpression, at least partially, preserved the mitochondrial respiration capacity and OXPHOS capacity in the myocardium stressed by chronic *Tc* infection.

Next, we determined whether MnSOD overexpression controlled the mtROS generation and established oxidant/antioxidant balance in chagasic heart. The plasma total antioxidant capacity (TAC) was decreased by 44.6% with progressive infection (Fig. 2A $^{*}p < 0.01$), and the levels of oxidative stress markers, that is, hydrogen peroxide (H_2O_2), protein carbonyls, and malondialdehyde (MDA), were increased by 9.1-fold, 3.5-fold, and 2.8-fold, respectively, in the myocardium of WT.*Tc* mice (*vs.* WT, all $^{*}p < 0.001$, Fig. 2B.a–c). Likewise, isolated cardiac mitochondria of WT.*Tc* (*vs.* WT) mice exhibited 60.8% and 72.7% decline in the TAC and MnSOD activity, respectively (Fig. 2C.a, b, $^{*}p < 0.001$), and 3.4-fold and 11.7-fold increase in carbonylation of mitochondrial proteins, determined by Western

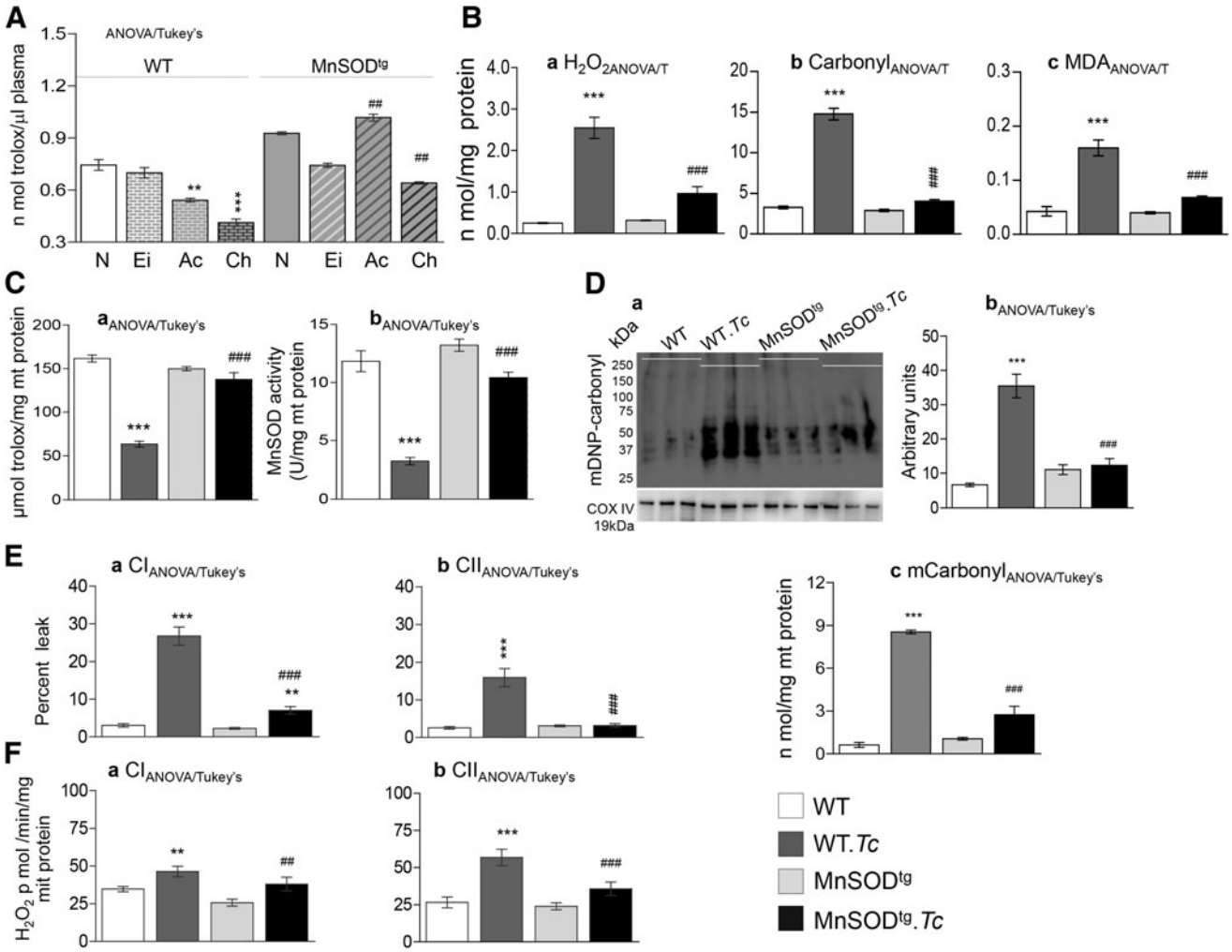

FIG. 2. Myocardial and mitochondrial antioxidant/oxidant imbalance and mtROS generation are decreased in MnSOD^{tg} mice infected with *T. cruzi*. C57BL/6 (WT and MnSOD^{tg}) mice were infected with *T. cruzi* and harvested at days 4 (early, Ei), 30 (acute, Ac), and 150 (chronic, Ch)pi. **(A)** Total antioxidant capacity in plasma of normal and infected mice was determined by Trolox assay. **(B)** Cardiac homogenates of chronically infected mice were utilized to monitor the H_2O_2 levels by an Amplex Red assay **(B.a)**, and protein carbonyls **(B.b)** and lipid hydroperoxides **(B.c)** by spectrophotometry assays. **(C–F)** Cardiac mitochondria from normal and chronically infected WT and MnSOD^{tg} mice were isolated by differential centrifugation. Isolated cardiac mitochondrial levels of antioxidant capacity **(C.a)**, MnSOD activity **(C.b),** and protein carbonyls determined by Western blotting **(D.a, D.b)** and spectrophotometry **(D.c)** are shown. Electron flow in isolated mitochondria was supported through CI and CII substrates. Shown are the mitochondrial electron leakage **(E.a, E.b)** and the rate of H_2O_2 production by an Amplex Red assay **(F.a, F.b).** Data are plotted as mean value ± SEM ($n = 6$–10 mice per group, triplicate observations per mouse). Significance is shown as $^{**,\#\#}p < 0.01$, and $^{***,\#\#\#}p < 0.001$. H_2O_2, hydrogen peroxide; mtROS, mitochondrial reactive oxygen species.

blotting and spectrophotometry, respectively (Fig. 2D.a–c, $^{*}p < 0.001$). The myocardial and mitochondrial antioxidant/oxidant imbalance was associated with a decline in mitochondrial health. Isolated cardiac mitochondria of WT.*Tc* (*vs.* WT) mice energized with CI and CII substrates exhibited a 7.8-fold and 5.1-fold increase in electron leakage, respectively (Fig. 2E.a, b, all $^{*}p < 0.001$), and a 33% and 114% increase in H_2O_2 release, respectively (Fig. 2F.a, b, all $^{**}p < 0.01$). The MnSOD^{tg} mice maintained the circulating TAC at all stages of infection and disease development at levels above or similar to that noted in normal WT controls (Fig. 2A), and effectively managed the chronic oxidative stress evidenced by only twofold increase in H_2O_2 level and no increase in protein carbonyls and MDA levels in the heart during disease phase (Fig. 2B.a–c). Furthermore, MnSOD^{tg} mice were equipped to maintain mitochondrial health evidenced by only a modest, but nonsignificant, increase in *Tc*-induced electron leakage, protein carbonyls, and H_2O_2 release (Fig. 2C–F, all, $^{\#\#}p < 0.01$).

We confirmed the positive effects of MnSOD overexpression on mitochondrial health during *Tc* infection by using an *in vitro* system. Cultured HeLa cells were transfected with pBI.EGFP–MnSOD (or pBI.EGFP only) and infected with *Tc* for 0–24 h. An even distribution of EGFP was noted in >50% of the transfected HeLa cells (Fig. 3A.a, b) and pBI.EGFP–MnSOD-expressing HeLa cells exhibited a 92% increase in mitochondrial MnSOD level, thus confirming that induced MnSOD was translocated to the

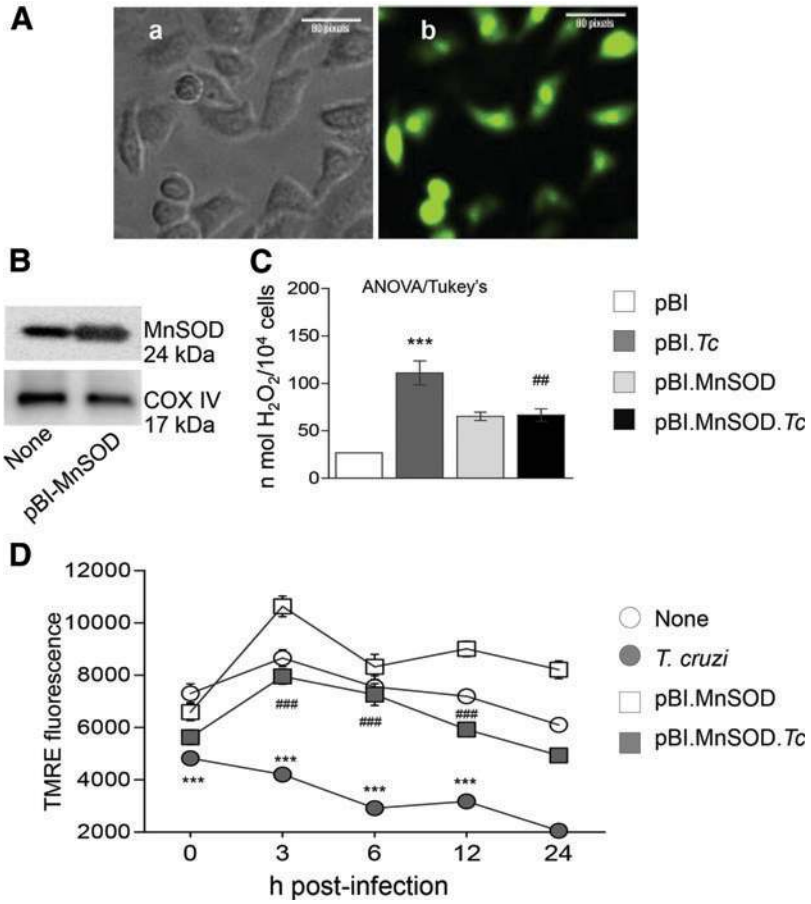

FIG. 3. ***T. cruzi*-induced ROS and mitochondrial defects are controlled in MnSOD-transfected cells.** HeLa cells were transfected with eukaryotic expression vector pBI.GFP–MnSOD. **(A)** Phase contrast **(A.a)** and UV epifluorescence **(A.b)** images showed that >50% of the HeLa cells were transfected and expressed EGFP-linked MnSOD. **(B)** Mitochondria were isolated from normal and pBI.GFP–MnSOD-transfected HeLa cells. Western blotting showed increased mitochondrial MnSOD level in transfected cells. **(C)** Normal and MnSOD-expressing HeLa cells were incubated with *T. cruzi* trypomastigotes (cell: parasite ratio, 1:5) for 24 h, and H_2O_2 release was determined by an Amplex Red assay. **(D)** Hela cells (normal and pBI.GFP–MnSOD transfected) were seeded in a 96-well plate, infected with *T. cruzi* for 1 h, washed to remove free parasites, and then loaded with TMRE. Cells were incubated for 0, 3, 6, 12, and 24 h. Shown are changes in TMRE fluorescence (detects changes in mitochondrial membrane potential) monitored as described in Materials and Methods section. Data are plotted as mean value ± SEM, and are representative of three independent experiments (triplicate observations per experiment). Significance was calculated and shown as described in Figure 1, and shown as $^{\#\#}p < 0.01$, $^{***,\#\#\#}p < 0.001$. TMRE, tetramethylrhodamine, ethyl ester. To see this illustration in color, the reader is referred to the web version of this article at www.liebertpub.com/ars

mitochondria in transfected cells (Fig. 3B). HeLa cells infected with *Tc* for 24 h exhibited a 2.2-fold increase in H_2O_2 release and the pBI.EGFP–MnSOD-expressing HeLa cells completely inhibited the *Tc*-induced H_2O_2 release (Fig. 3C). The mitochondrial membrane potential, determined by using the tetramethylrhodamine, ethyl ester (TMRE) fluorescence probe, was gradually decreased by 34–66% in Hela cells during 0–24 h pi (Fig. 3D, $^{***}p < 0.001$). In comparison, pBI.EGFP–MnSOD-transfected Hela cells infected with *Tc* for 0–24 h maintained the TMRE fluorescence similar to that noted in normal cardiomyocytes (Fig. 3D). Together, the results presented in Figures 2 and 3 suggested that (a) MnSOD overexpression preserved the antioxidant/oxidant balance that otherwise was tipped toward damaging oxidants in the myocardium of chagasic mice and *Tc*-infected cells and (b) these benefits of MnSOD overexpression were delivered by preservation of mitochondrial membrane potential thereby inhibiting the electron leakage and ROS generation through mitochondrial electron transport chain in the myocardium of chronically infected mice and *Tc*-infected cells.

We then determined why antioxidant response is downregulated in chagasic heart, and how MnSOD overexpression, besides enhancing the mtROS scavenging capacity, improved the antioxidant response. NFE2L2 is a major transcription factor that regulates the expression of antioxidant proteins. Western blotting showed ≥twofold decline in the expression and nuclear translocation of NFE2L2 in chagasic myocardium (Fig. 4A.a–d, $^{*}p < 0.001$). No change in the expression of Kelch-like ECH-associated protein (Keap1; inhibits NFE2L2 activity) was noted in any of the groups (Fig. 4B.a, b). Instead, NFE2L2 binding to ARE sequences located in the regulatory region of multiple genes encoding for phase II detoxification enzymes and antioxidant proteins was decreased by 52% in the

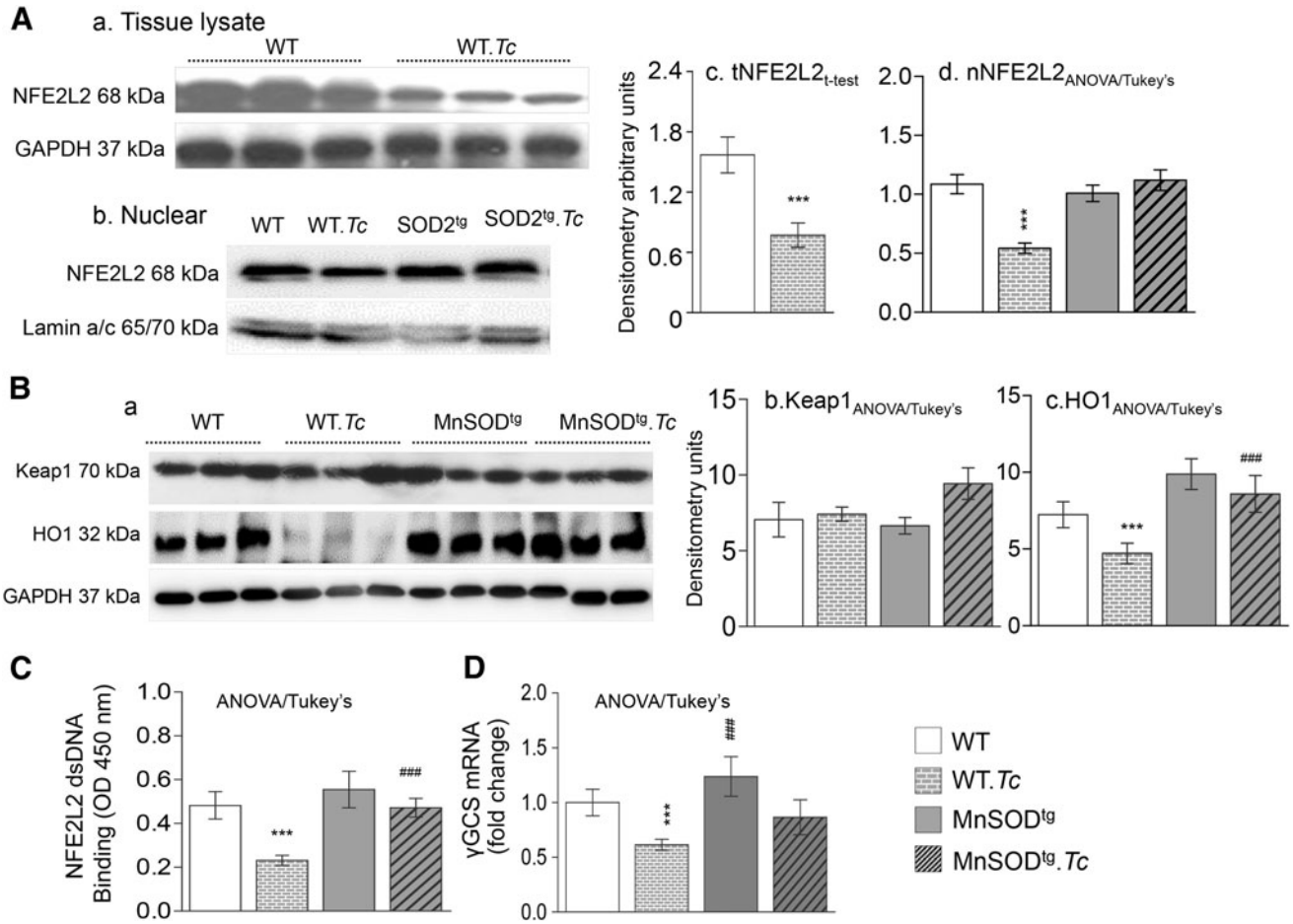

FIG. 4. NFE2L2 transcriptional activation in chagasic myocardium (±MnSOD). Mice were infected with *T. cruzi* and harvested at 150 days pi. **(A)** Western blotting. Heart tissue homogenates **(A.a, A.c)** and nuclear fractions **(A.b, A.d)** were subjected to Western blotting with anti-NFE2L2 antibody **(A.a, A.b)**, and densitometry analysis of the NFE2L2 signal **(A.c, A.d)** is presented. **(B)** Western blotting and densitometry analyses of Keap1 **(B.a, B.b)** and HO1 **(B.a, B.c)** levels in heart homogenates. Densitometry analysis of WB bands in heart homogenates and nuclear fractions were normalized to GAPDH and Lamin A/C, respectively. **(C)** NFE2L2–ARE binding. NFE2L2 double-stranded (ds) DNA-binding capacity in nuclear fractions of heart tissue from WT and MnSOD^{tg} mice (±*Tc*) was measured as described in Materials and Methods section. **(D)** RT-qPCR analysis for γGCS mRNA level in WT and MnSOD^{tg} mice (±*Tc*). Data are plotted as mean value ± SEM ($n = 6$–10 mice per group). Significance is shown as $^{***,\#\#\#}p < 0.001$. ARE, antioxidant response element; γGCS, gamma-glutamyl cysteine synthase; HO1, heme oxygenase-1; Keap1, Kelch-like ECH-associated protein 1; mRNA, messenger RNA; NFE2L2, nuclear factor (erythroid 2)-like 2; RT-qPCR, real-time quantitative polymerase chain reaction.

myocardium of WT.*Tc* (*vs.* WT) mice (Fig. 4C, $^{*}p < 0.001$). Subsequently, a 30–38% decline in MnSOD (Supplementary Fig. S1A) and γGCS (Fig. 4D) mRNA levels and HO1 protein level (Fig. 4B.a, c) was noted in the myocardium of WT.*Tc* (*vs.* WT, $^{*}p < 0.001$) mice. The MnSOD^{tg}.*Tc* mice exhibited no decline in nuclear translocation of NFE2L2 (Fig. 4A.b, d) and NFE2L2–ARE binding capacity (Fig. 4C), and consequently, mRNA for MnSOD (Supplementary Fig. S1A) and γGCS (Fig. 4D), and HO1 protein level (Fig. 4B.a, d) were preserved in MnSOD^{tg}.*Tc* mice to the levels detected in WT controls. These results suggested that MnSOD prevented the mtROS disturbance of NFE2L2-dependent antioxidant response in chagasic myocardium.

We confirmed the role of MnSOD induction of NFE2L2 during *Tc* infection by using an *in vitro* system. Cardiomyocytes (normal and pBI.EGFP–MnSOD-transfected) were infected with *Tc* for 24 h, stained with NFE2L2-conjugated Alexa Fluor 568 (red) and 2-(4-amidinophenyl)-1H-indole-6-carboxamidine (DAPI, binds nucleus, blue), and analyzed by confocal fluorescence microscopy (Fig. 5A). In response to *Tc* infection, cytosolic and nuclear levels of NFE2L2 fluorescence were decreased in cardiomyocytes transfected with empty plasmid (Fig. 5A, compare Fig. 5A.a–c *vs.* Fig. 5A.d–f), but were maintained to normal levels in pBI.EGFP–MnSOD-expressing cells (Fig. 5A, compare Fig. 5A.g–i *vs.* Fig. 5A.j–l). Real-time (RT)-quantitative PCR showed that the mRNA level for NFE2L2 was equally decreased in response to *Tc* infection in control and pBI.EGFP–MnSOD-expressing cells (Fig. 5B.a, $^{*}p < 0.01$). The mRNA levels for NFE2L2-dependent glutamate-cysteine ligase modifier subunit (GCLM), thioredoxin (Trx), GST, and NQO1 antioxidants were depressed by 100%, 72.9%, 41.6%, and

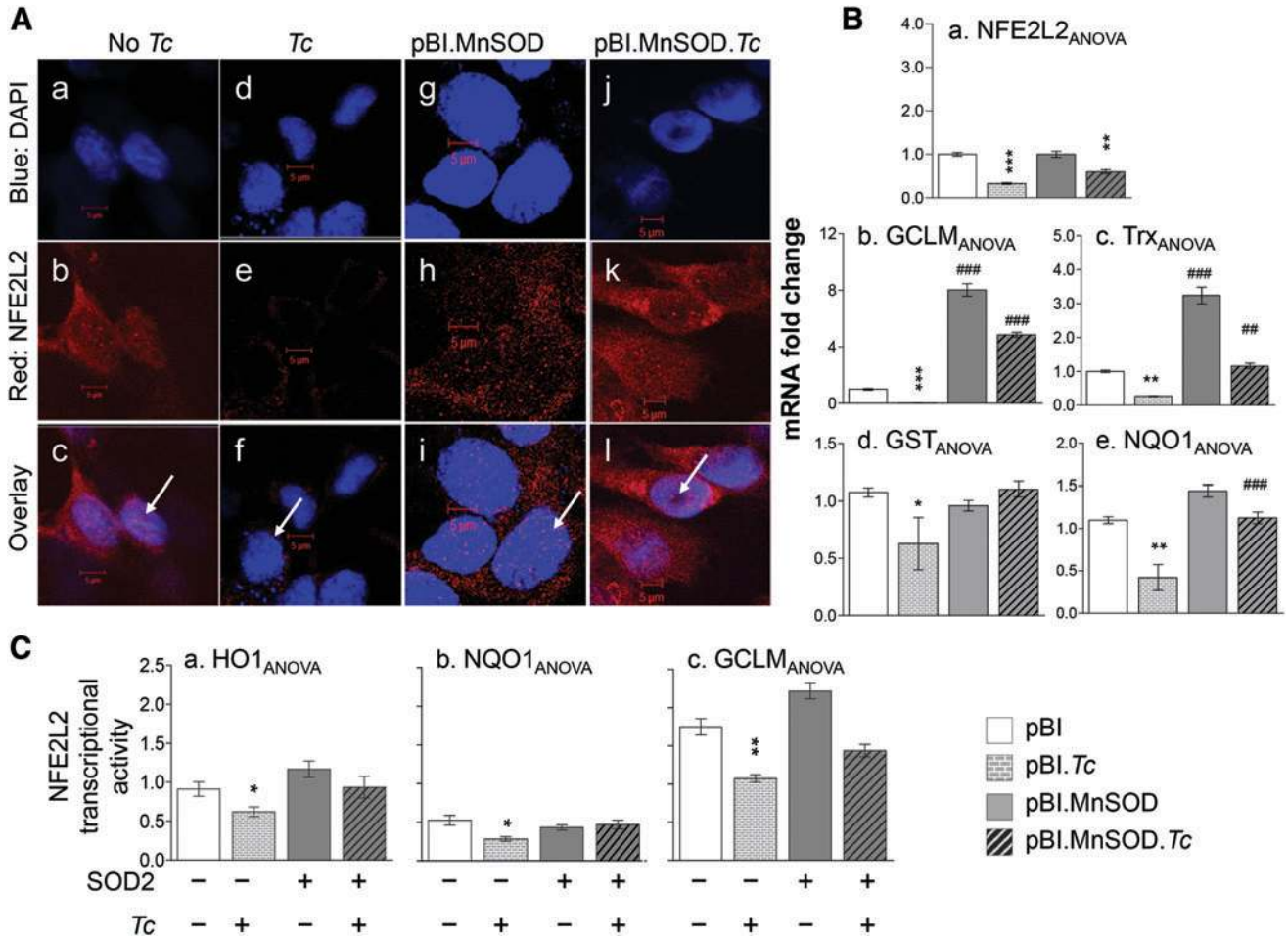

FIG. 5. MnSOD preserves NFE2L2–ARE functional activity in *Tc*-infected cells. **(A)** Confocal microscopy. Cardiac myocytes were transfected with empty vector **(A.a–A.f)** or pBI.EGFP–MnSOD **(A.g–A.l)** and incubated with **(A.d–A.f, A.j–A.l)** or without **(A.a–A.c, A.g–A.i)** *T. cruzi* for 24 h. Cells were stained with DAPI (*nuclear blue*, **A.a, A.d, A.g, A.j)** and Alexa Fluor 568-conjugated anti-NFE2L2 antibody (*red*, **A.b, A.e, A.h, A.k**) and analyzed by confocal fluorescence microscopy. Overlay images **(A.c, A.f, A.i, A.l)** show cytosolic and nuclear localization of NFE2L2. **(B)** Antioxidant genes' expression. RT-qPCR measurement of mRNA levels for **(B.a)** NFE2L2, **(B.b)** GCLM, **(B.c)** Trx, **(B.d)** GST, and **(B.e)** NQO1 in cardiomyocytes transfected with MnSOD expression plasmid and infected with *T. cruzi* for 24 h. Fold change was determined after normalizing the data with GAPDH mRNA. **(C)** NFE2L2 transcriptional activity. HeLa cells were transiently transfected with pGL3-promo-2x-hHO1 **(C.a)**, pGL3-promo-2x-hNQO1 **(C.b)**, or pGL3-promo-2x-hGCLM **(C.c)** plasmids consisting of luciferase encoding gene under NFE2L2-binding ARE sequence from HO1, NQO1, and GCLM, respectively. Cells were cotransfected with an MnSOD-expressing plasmid and a Renilla luciferase plasmid (positive control for normalization of transfection efficiency). Transfected cells were infected (cell:*Tc*ratio, 1:5) for 24 h. The relative NFE2L2 transcriptional activity for HO1, NQO1, and GCLM was measured by using a dual luciferase assay and normalized to Renilla luciferase activity. Data (mean ± SEM) are representative of three independent experiments (triplicate observations per experiment). Significance is shown as $*p<0.05$, $**,^{\#\#}p<0.01$, $***,^{\#\#\#}p<0.001$. GCLM, glutamate-cysteine ligase modifier subunit; GST, glutathione S transferase; NQO1, NAD(P)H dehydrogenase, quinone 1; Trx, thioredoxin. To see this illustration in color, the reader is referred to the web version of this article at www.liebertpub.com/ars

61.6%, respectively, in *Tc*-infected control cells (Fig. 5B.b–e, $*p<0.05$). The pBI.EGFP–MnSOD-transfected cardiomyocytes exhibited sevenfold, threefold, and 44% higher levels of mRNA for GCLM, Trx, and NQO1, respectively, than the pBI-transfected control cells (Fig. 5B.b, c, e). The mRNA levels for GCLM, Trx, GST, and NQO1 antioxidants in MnSOD-expressing cardiomyocytes infected with *Tc* remained significantly higher or equal to that noted in pBI-transfected control cells (Fig. 5B.b–e, $^{\#}p<0.01$). To demonstrate that the increase in antioxidants expression was indeed because of an increase in NFE2L2 activity, we transfected the control and MnSOD-expressing HeLa cells with pGL3-promo-2x-hHO1, pGL3-promo-2x-hNQO1, and pGL3-promo-2x-hGCLM plasmids encoding luciferase gene under the NFE2L2-binding ARE sequences from HO1, NQO1, and GCLM, respectively, and then infected with *Tc* for 24 h. These results showed that *Tc* infection resulted in 32%, 46%, and 39% decline in HO1, NQO1, and GCLM promoter-dependent luciferase activity (normalized to Renilla luciferase), respectively (Fig. 5C.a–c, $*p<0.05$–0.01). Cotransfection with pBI.EGFP–MnSOD plasmid arrested the *Tc*-induced decline in NFE2L2 transcriptional activity

(Fig. 5C.a–c). Taken together, the results presented in Figures 4 and 5 suggested that (a) *Tc*-induced mtROS suppressed the NFE2L2 nuclear translocation, binding with AREs, and transcriptional activity resulting in a compromised antioxidant response in cardiac myocytes, Hela cells, and chagasic heart. Furthermore, (b) MnSOD overexpression was beneficial in preserving the NFE2L2 transcriptional activity and NFE2L2-dependent antioxidant expression in *Tc*-infected cells and myocardium of chagasic mice.

To determine whether preservation of NFE2L2-regulated antioxidant status improved the cardiac performance in chagasic mice, we performed transthoracic ECG (Fig. 6 and Supplementary Table S1). These data showed that the LV systolic function, that is, stroke volume (SV), cardiac output (CO), and ejection fraction (EF) were decreased by 50%, 61%, and 45%, respectively (Fig. 6a–c, $*p<0.001$), and end systolic volume (ESV) was increased by 100% (Fig. 6d, $*p<0.001$) in WT.*Tc* (*vs*. WT) mice. A significant increase in LV internal diameter (LVID-s: 117%) and consequent decline in fractional shortening (FS; 63%, Supplementary Table S1, $*p<0.001$) further suggested that compromised contraction contributed to decreased LV systolic function in WT.*Tc* mice. The pulse wave Doppler ECG showed that the transmittal flow of blood from left atrium to LV through mitral valve was decreased by 37% during early peak (E, Fig. 6e, $*p<0.001$) and increased by 78% during late peak (A, Fig. 6f, $*p<0.001$) in chagasic myocardium. The prolonging of isovolumic contraction time (IVCT; 85% increase, Fig. 6g) and isovolumetric relaxation time (IVRT; 47% increase, Fig. 6h) and a shortening of LV ejection time (LVET) indicated poor myocardial performance index (all, $*p<0.001$, Supplementary Table S1) in chagasic WT mice. In comparison, chronically infected MnSOD^{tg} mice preserved the LV systolic function to the normal level (Fig. 6a–d), improved the diastolic performance by >50% (Fig. 6e–h), and *Tc*-induced changes in LVID-s, FS, and LVET were not completely eliminated (Supplementary Table S1). Together, these results suggested that (a) LV systolic function and diastolic

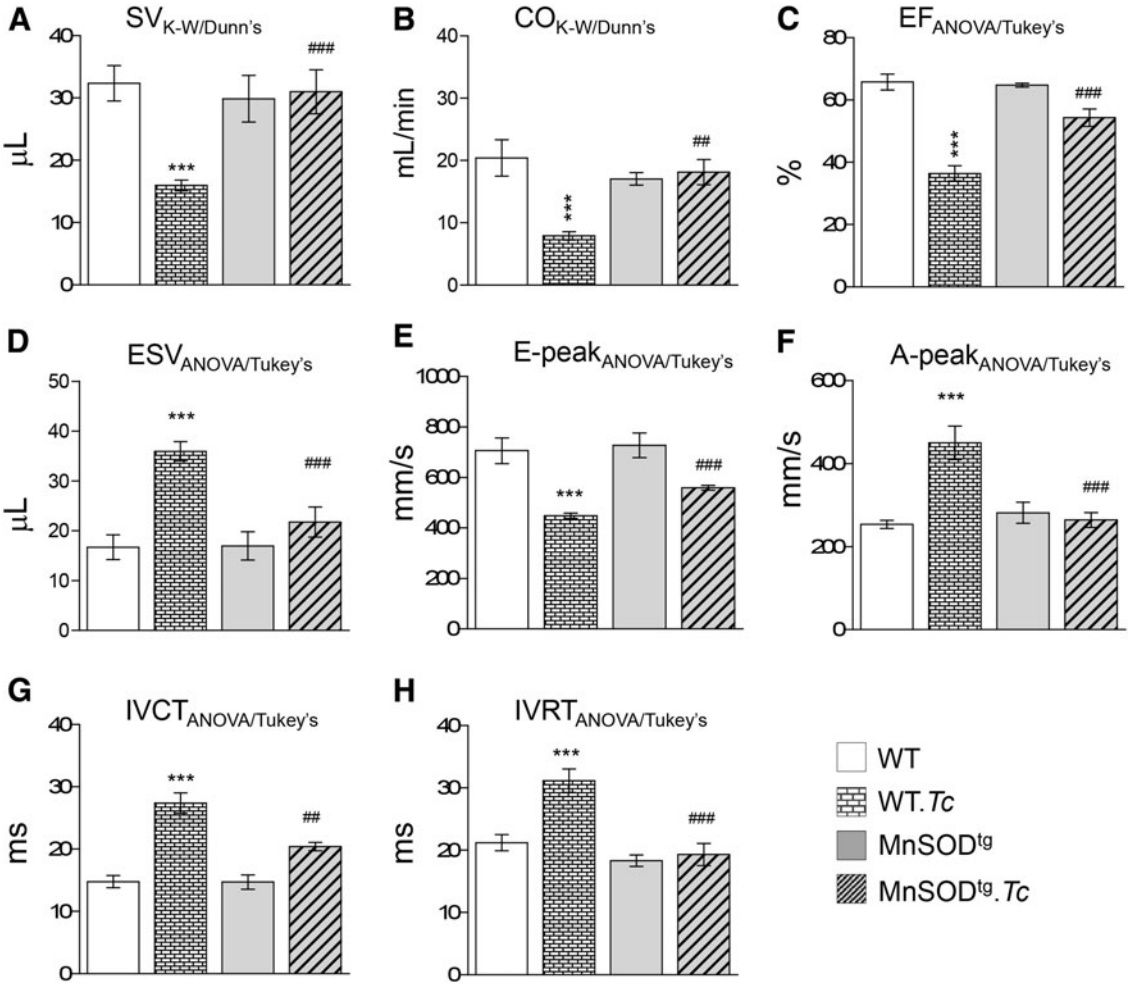

FIG. 6. Left ventricular systolic and diastolic performance in chagasic mice (±MnSOD). C57BL/6 female mice (WT and MnSOD^{tg}) were infected with *Tc*. Shown are transthoracic echocardiography measurements of **(A)** SV, **(B)** CO, **(C)** EF, and **(D)** ESV in mice at ≥120 days pi. Pulse wave Doppler echocardiography was performed to measure mitral valve **(E)** early and **(F)** late peak velocities, **(G)** IVCT, and **(H)** IVRT in chagasic mice. Data are plotted as mean value ± SEM ($n=6$–10 mice per group, triplicate observations per mouse). Significance is shown as $^{\#\#}p<0.01$, and $***,^{\#\#\#}p<0.001$. Detailed data are presented in Supplementary Table S1. CO, cardiac output; EF, ejection fraction; ESV, end systolic volume; IVCT, isovolumic contraction time; IVRT, isovolumetric relaxation time; SV, stroke volume.

performance were compromised in chronically infected WT mice and (b) MnSOD/NFE2L2-dependent improvement in mitochondrial health and antioxidant/oxidant balance restored the LV hemodynamics during chronic infection.

To gain an anatomopathological view of the heart, we took a measure of LV walls, and also performed histological and molecular studies. ECG imaging showed the interventricular septum (IVS) thickness (Fig. 7A.a, b) and LV area (Fig. 7A.c, d) during systolic and diastolic phases, as well as the LV mass (Fig. 7e) was increased by 43–74% (all, $*p<0.001$), whereas LV posterior wall (LVPW) was thinned (Fig. 7A.f, $*p<0.01$) in chagasic WT mice (Supplementary Table S1). Histological evaluation of tissue sections by Masson's Trichrome staining showed that the myocardial collagen content, specifically around the vasculature, was markedly increased in chagasic myocardium (score: 4.0 ± 0.4 *vs*. 0.3 ± 0.04, WT.*Tc vs*. WT, $*p<0.001$, Fig. 7B). An increase in cardiac fibrosis in WT.*Tc* mice was also evidenced by 7-fold, 11-fold, 2-fold, 2.4-fold, and 2.4-fold increase in mRNA levels for COLI, COLIII, COLV, αSMA, and αSM22, respectively (Fig. 7C.a–e, all, $*p<0.001$). In MnSOD^{tg}.*Tc* mice, although IVS-s thickness and LV area-d remained higher than normal levels (Fig. 7A.a, d, $p<0.01$), LV area-s, LVPW-s, and LV mass (Fig. 7A.c, e, f) were maintained to the levels noted in matched (MnSOD^{tg}) and WT controls. The control of *Tc*-induced fibrosis in MnSOD^{tg} mice was also evidenced by a significant decline in collagen deposition (Fig. 7B, score: 2 ± 0.26), 51–94% decline in collagen-related gene expression (Fig. 2C.a–c), and normal levels of αSMA and αSM22 expression (Fig. 7C.d–e, all, $^{\#}p<0.001$). Together these results suggested that changes in the LV walls' thickness (and thereby contractile capacity) contributed to compromised systolic and diastolic performance of the heart in chagasic mice. The benefits of MnSOD/NFE2L2 in preserving LV hemodynamics (Fig. 6) were delivered *via* preservation of IVS and LVPW flexibility through control of cardiac collagenosis (Fig. 7) in chagasic disease.

Finally, we determined whether *Tc*-induced heart dysfunction was correlated with parasite burden. We obtained a quantitative measure of tissue parasite burden by PCR amplification of *Tc*18srDNA. The primer pairs were confirmed to produce a single amplicon by traditional PCR and RT-PCR (Supplementary Fig. S3A) and all samples produced a signal

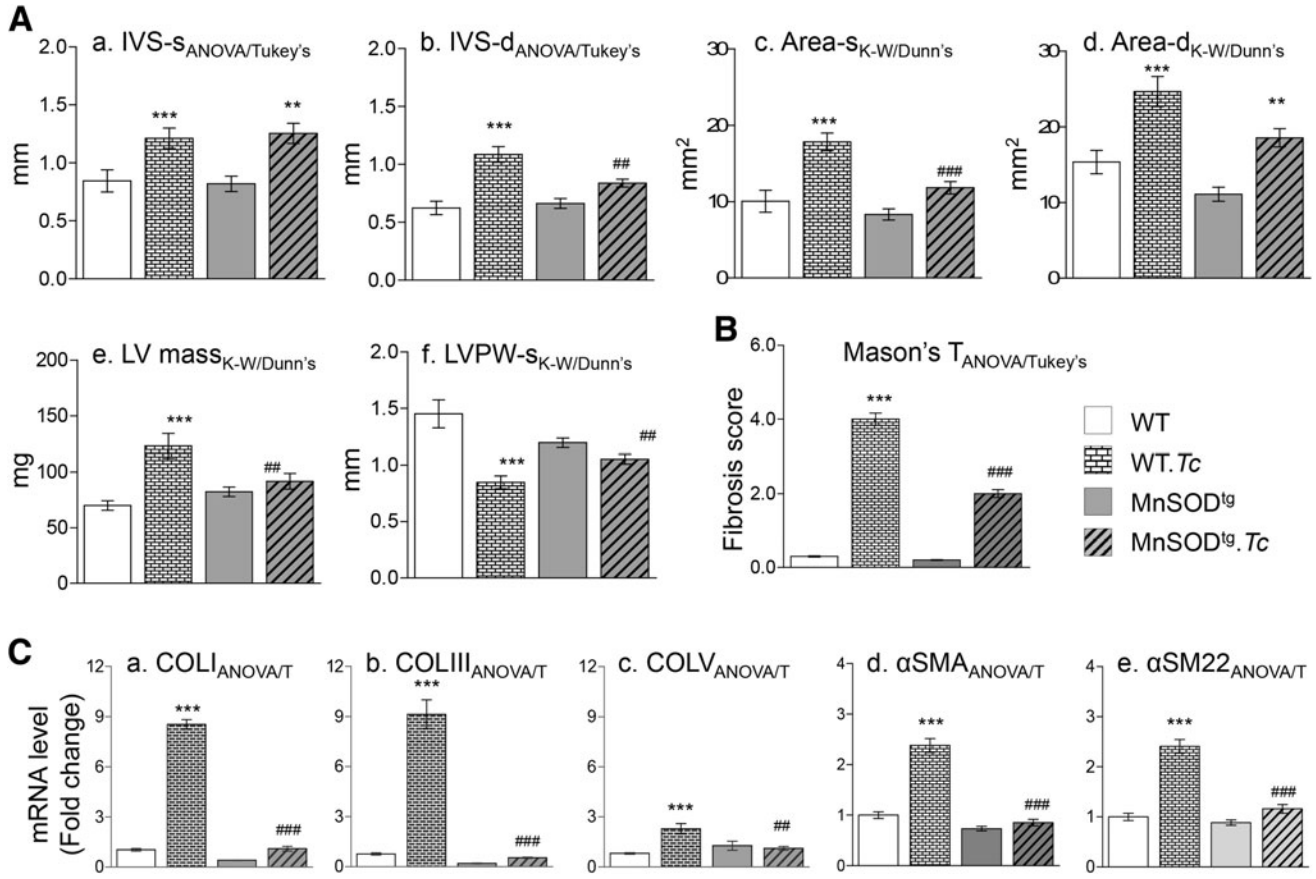

FIG. 7. Cardiac remodeling in chagasic mice (±MnSOD). Mice (WT and MnSOD^{tg}) were infected as shown in Figure 6. **(A)** Cardiac structural changes were analyzed by echocardiography using a Vevo 2100 system. Shown are systolic (-s) and diastolic (-d) values for IVS thickness **(A.a, A.b)**, LV area **(A.c, A.d)**, LV mass **(A.e),** and LVPW thickness **(A.f)** in chronically infected mice. **(B)** Fibrosis score. Heart tissue sections of chronically infected WT and MnSOD^{tg} mice were stained with Mason's trichrome, and tissues were scored for collagen as described in Materials and Methods section. **(C)** Gene expression analysis. RT-qPCR was performed to evaluate mRNA levels for collagen isoforms COLI, COLIII, and COLV **(C.a–C.c)**, αSMA **(C.d)** and αSM22 **(C.e)**. Data are plotted as mean value ± SEM ($n=6$–10 mice per group, triplicate observations per mouse). Significance is shown as $**,^{\#\#}p<0.01$, and $***,^{\#\#\#}p<0.001$. IVS, inter-ventricular septum; LV, left ventricle; LVPW, LV posterior wall.

within the standard curve range (Supplementary Fig. S3B). Pearson's correlation analysis of tissue levels of *Tc*18SrDNA *versus* changes in percentage EF in chagasic WT and $MnSOD^{tg}$ mice identified no significant correlation between parasite burden and EF in WT and $MnSOD^{tg}$ mice (Supplementary Fig. S3C, D). These results confirmed that parasite persistence in chronically infected host is not the only factor to cause heart dysfunction.

Discussion

Our data from this study and other reports [reviewed in Tanowitz *et al.* (47)] have suggested that a pro-oxidant milieu is presented in the myocardium and may be of pathological importance in progressive development of CCM. However, the mechanism(s) of oxidative stress generation and its role in disease pathology are not known. In this study, we provide the first direct evidence that (a) *in vivo* OXPHOS capacity is compromised in chagasic myocardium and contributes to mtROS production and (b) mtROS inhibited the nuclear translocation and transcriptional activation of NFE2L2-dependent antioxidant gene expression. Because of the host's inability to arrest ROS, (c) extensive oxidative adducts and cardiac remodeling led to compromised systolic and diastolic performance of the chagasic heart. By using $MnSOD^{tg}$ mice, we found that MnSOD-dependent scavenging of the ROS (d) halted the loss in mitochondrial oxidative metabolism and NFE2L2 transcriptional activity. Importantly, (e) MnSOD/NFE2L2 protection from oxidative stress was beneficial in arresting the chronic cardiac remodeling and LV dysfunction in chagasic hearts. To the best of our knowledge, this is the first report demonstrating a molecular link between mtROS and NFE2L2 transcriptional activity and their mechanistic role in the development of chronic cardiomyopathy and left ventricular systolic and diastolic dysfunction in Chagas disease.

MnSOD is a primary antioxidant enzyme in mammalian cells catalyzing the conversion of two molecules of superoxide anion ($O_2^{\bullet -}$) generated either as by-products of mitochondrial OXPHOS or under oxidative stress into H_2O_2, which is further oxidized to water. MnSOD significantly reduces drug-induced cardiac injury through protecting mitochondria from damage caused by superoxide radicals (58). In the context of CCM, decreased myofibrillar OXPHOS capacity (Fig. 1 and Supplementary Fig. S2) along with increased mtROS production (Fig. 2) contributed to oxidative adducts (Figs. 2 and 3), and MnSOD overexpression rescued the mitochondrial function in chagasic myocardium (Fig. 1) as well as *in vitro* cultured HeLa cells and cardiac myocytes infected by *Tc* (Fig. 3). Our findings confirm that MnSOD/mtROS interplay determines the extent of oxidative adducts of the macromolecules such as DNA, lipids, and proteins observed in the myocardium of chagasic mice (Fig. 2) (14, 52), rats (55), and humans (10, 57).

To ameliorate oxidative injury and maintain redox homeostasis, mammals have developed an efficient defense system of enzymatic and nonenzymatic antioxidants. How *Tc* signals MnSOD inefficiency of gene/protein expression and activity and why host is not able to activate the antioxidant response to mtROS stress are not known. MnSOD is transcriptionally regulated through multiple transcription factors, including SIRT1/FOXO3a (31, 33, 36), MEK/ERK/NF-κB (3), and peroxisome proliferator-activated receptor γ (PPARγ) (15). A pronounced activation of NF-κB (4), AP1 (27), and PPARs (26) has been noted in various models of *Tc* infection; however, activation of these transcriptional factors did not correlate with MnSOD expression (Supplementary Fig. S1) in Chagas disease. These observations suggest that the expression and activation of MnSOD and other antioxidants in the context of Chagas disease are regulated through other transcription factors.

NFE2L2 is a basic leucine zipper transcription factor that binds to the AREs in the promoter region of the antioxidant genes (39, 51). Many oxidants, heavy metals, phenolic antioxidants, and GSH-conjugating agents serve as inducers of NFE2L2 in regulation of the antioxidant gene expression (51). However, despite an increase in oxidative stress (Figs. 2 and 3), *Tc*-infected cardiac myocytes and HeLa cells (Figs. 3 and 5) and murine hearts [Fig. 4 (38)] showed decreased expression of γGCS required for GSH synthesis and of antioxidant enzymes (*e.g.*, GCLM, GST, Trx, HO1, NQO1). Our findings of decreased nuclear translocation and transcriptional activity of NFE2L2 in *Tc*-infected HeLa cells, cardiac myocytes, and myocardium of chagasic mice that were ameliorated by MnSOD overexpression (Figs. 4 and 5) suggest that mtROS, instead of a stimulator, inhibited the NFE2L2 activity during *Tc* infection. *T. cruzi* may influence the mtROS generation and NFE2L2 activation through independent pathways, or *Tc*-induced mtROS may alter the NFE2L2 stability and nuclear translocation. It is also possible that mtROS alters the binding of NFE2L2 with other partners, for example, Keap1 [a negative regulator of NFE2L2 (49)] or PGC1α [a cofactor required for NFE2L2 transcriptional activation (5)], or oxidative modifications result in the assembly of a transcriptionally inactive complex, and this remains to be investigated in future studies.

Various modalities of ECG provide useful structural and functional information in the detection of early myocardial damage, risk assessment of prognosis, disease progression, and management of heart condition (1). In chagasic patients, the heart is dilated, LV systolic and diastolic functions are usually abnormal with advanced clinical heart failure, and many of them present LV apical and other segmental wall abnormalities (2, 37, 41). We performed detailed evaluation of LV structure, contractile function, and blood flow by ECG to establish whether our experimental model captures the cardiac changes as observed in chagasic patients, and also obtained a molecular basis for the observed changes in the heart. Transthoracic ECG showed that an increase in IVS thickness and LV stiffness (increased LV mass) along with enlargement of the heart (increase in LV area, thinning of LVPW) was associated with the development of systolic LV dysfunction in WT chagasic mice (Figs. 6 and 7). Molecular and histological studies demonstrated increased expression of the profibrotic genes and collagen deposition in chagasic myocardium (Fig. 7). The phenotypic transformation of fibroblasts to myofibroblasts, triggered by ROS release, contributes to fibrosis, collagenosis, and the activation of matrix metalloproteinases involved in the remodeling of the failing myocardium (17). ROS-dependent formation of advanced glycation end (AGE) products is recognized as an underlying mechanism for accelerated cross-linking of collagens in aging and diabetes (32, 40), and may also be relevant in CCM. Furthermore, hyperplasia and migration of cardiac fibroblasts to the interstitial space are facilitated by growth factors (*e.g.*,

fibroblast growth factor and TGF-β) and fibrogenic cytokines (*e.g.*, IL-1β and TNF-α), all of which are enhanced in chagasic myocardium [reviewed in Machado *et al.* (35)]. This results in an increase in collagen content and also in structural changes in collagen network, causing abnormal stiffness and pressure overload. Carvedilol maintains cross-linking, reduces cardiac workload and oxygen consumption, peripheral vasodilation, and cellular apoptosis, and works as a potent antioxidant (9, 18). Indeed, adding carvedilol to enalapril (ACE inhibitor) and spironolactone (reduces fluid retention) therapy was beneficial in improving EF in chagasic patients (9, 18). Thus, we surmise that (a) our experimental model of chronic *Tc* infection captures the abnormalities of LV systolic function as is noted in chagasic patients and (b) mtROS/NFE2L2 imbalance and consequent signaling of fibrotic gene expression constitute a key mechanism in the development of CCM.

Besides hypertrophy, that is, pathological thickening of the LV walls, myocardial injury impairs ventricular relaxation and diastolic filling (6, 24). The mitral inflow reflects the pressure difference between the atria and the ventricle, and any abnormality of diastolic pressure in the chambers affects the velocity and shape of the Doppler inflow signal. Specifically, diastolic dysfunction alters the relationship between early and late filling (E- and A-wave), and the length of the IVRT. In a healthy heart, the E velocity (early peak of blood flow from left atrium to LV) is greater than the A velocity (late peak of blood flow with atrial contraction). In a recent study, $Nrf2^{+/-}$ mice were reported to preserve the systolic function, but developed impaired LV diastolic function with prolonged E wave, mitral valve ejection time (MVET), IVRT, and increased myocardial perfusion index (MPI) associated with cardiac hypertrophy and nonresponsiveness to pharmacological modulators of Ca^{2+} homeostasis (*e.g.*, isoproterenol) (16). In our study, chronically infected mice exhibited reduced LV compliance evidenced by a significant decline in E wave, increase in A wave, and E/A ratio = 1 (normal E/A ratio >2.0), suggesting reduced filling of the LV in the period between contractions (19). The prolonging of IVCT and IVRT but a shortening of MVET indicated poor inflow of blood and relaxation of the heart (8) as well as decreased ability to maintain contraction for ejection of the oxygenated blood. Enhancing the MnSOD/NFE2L2 improved the LV E/A ratio and relaxation, and myocardial performance index in chagasic mice, suggesting that the ROS-induced hypertrophy and cardiac injuries contribute to impaired myocardial relaxation and diastolic dysfunction in CCM.

Materials and Methods

Mice, parasites, and cell culture

C57BL/6 mice (WT) were purchased from Harlan Laboratories (Indianapolis, IN). $MnSOD^{tg}$ mice (C57BL/6 background) were kindly provided by Dr. H. Van Rammen (30, 34). All mice were bred at the University of Texas Medical Branch (UTMB) animal facility. *T. cruzi* SylvioX10/4 isolate and C2C12 murine skeletal muscle cell line were purchased from ATCC (Manassas, VA). *T. cruzi* trypomastigotes were propagated by *in vitro* passage in C2C12 cells. Female mice (6 weeks old, body weight: 18.23 ± 1.67 g) were infected with *T. cruzi* (10,000 trypomastigotes/mouse, intraperitoneal) and harvested at days 4–7, 35–40, and 120–150 pi corresponding to phases of early invasion and dissemination, acute (peak) parasitemia, and chronic disease, respectively. Sera/plasma and tissue samples were stored at 4°C and −80°C, respectively. Human cardiac myocyte culture was maintained in Dulbecco's modified Eagle's medium (DMEM)/F-12 medium containing 12.5% fetal bovine serum (FBS). Human cervix epithelial cell line (HeLa, ATCC) was propagated in DMEM supplemented with Earle's salts, 2 m*M* L-glutamine, and 10% FBS. Protein level in all samples was determined by using the Bradford Protein Assay (Bio-Rad, Hercules, CA). All animal experiments were performed according to the National Institutes of Health Guide for Care and use of Experimental Animals, and were approved by the Institutional Animal Care and Use Committee at the UTMB, Galveston (protocol No. 805029).

Plasmids and transient transfection

The eukaryotic plasmids pBI.EGFP–MnSOD (CMV promoter; Addgene, Cambridge, MA) (44) and pRL.SV40 (Promega, Madison, WI) express full-length MnSOD and Renilla luciferase, respectively. The luciferase reporter plasmids, pGL3-promo-2x-hHO1, pGL3-promo-2x-hGCLM, and pGL3-promo-2x-hNQO1, were kindly provided by Dr. Sepppo Tiä-Herttuala (A.i. Virtanen Institute at University of Eastern Finland). For this, two promoter regions including NFE2L2-ARE sequences from human hemoxygenase (HO1), GCLM, and NADPH dehydrogenase quinone 1 (NQO1) were cloned in tandem into the pGL3 vector upstream of the SV40 minimal promoter and luciferase sequences (28). All recombinant plasmids were transformed into *Escherichia coli* DH5α-competent cells, grown in L-broth containing appropriate antibiotics (100 μg/ml), and purified using the Plasmid DNA Maxi Prep kit (Qiagen, Chatsworth, CA).

To measure the transfection efficiency, HeLa cells (10^4/well) were seeded in Lab-Tek II eight chamber slide and incubated overnight in antibiotic-free Opti-MEM. The pBI.EGFP–MnSOD plasmid was mixed with transfection reagent (100 ng DNA in 5 μl H_2O and 0.3 μl Lipofectamine 2000; Invitrogen, Carlsbad, CA) and added to the well. After 6 h of incubation, cells were washed, replenished with complete medium for 3–5 h, and transfection efficiency was detected by recording EGFP fluorescence at Ex_{488nm}/Em_{509nm} using ECLIPSE Ti inverted microscope with a 40× lens (Nikon, Melville, NY).

Genotyping and tissue parasite burden

Tail biopsies (2–3 mm) from young pups or heart tissue sections (10 mg) from WT and $MnSOD^{tg}$ mice, with or without *T. cruzi* infection, were subjected to Proteinase-K lysis and total DNA was extracted by phenol/chloroform extraction/ethanol precipitation method. Total DNA was treated with RNase A (DNase and protease-free, Cat. No. EN0531 from Thermo Scientific, Waltham, MA) and purified by using DNeasy Mini Spin Columns (Qiagen, Germantown, MD). Total DNA absorbance was recorded at 260 and 280 nm by using a DU® 800 UV/Visible Spectrophotometer, and DNA concentration ($[OD_{260}–OD_{320}]\times 50$-$\mu$g/ml) and purity ($OD_{260}/OD_{280}$ ratio of 1.7–2.0) were recorded. Tail DNA samples were analyzed by traditional PCR for genotyping WT and $MnSOD^{tg}$ mice as described (43). Total DNA isolated from heart tissues (100 ng) was subjected to an RT qPCR on an iCycler thermal cycler with SYBR Green Supermix (Bio-Rad) and *Tc*18SrDNA-specific primers

(Supplementary Table S2), and fold change was calculated as $2^{-\Delta\Delta Ct}$, where ΔC_t represents the C_t (*Tc*18SrDNA) − C_t (GAPDH), and $\Delta\Delta C_t$ represents the ΔC_t for sample and − ΔC_t for control (22).

Gene expression analysis

Freshly harvested heart tissue sections (10 mg) from chronically infected and control (WT and $MnSOD^{tg}$) mice were snap frozen in liquid nitrogen and homogenized in TRIzol reagent (Invitrogen; weight/volume ratio, 1:10). Total RNA was extracted and precipitated by chloroform/isopropanol/ethanol method. The DNA that might be contaminating the RNA preparation was removed by RNase-free DNase I (New England Biolabs, Beverly, MA) treatment. Total RNA was analyzed by using a DU 800 UV/Visible Spectrophotometer (Beckman Coulter, Pasadena, CA) to assess the quality ($OD_{260/280}$ ratio ≥2.0) and quantity (OD_{260} of 1 = 40 μg/ml RNA). Total RNA (2 μg) was reverse transcribed by using poly (dT)18 oligonucleotide with an iScript™ kit (Bio-Rad). The complementary DNA (cDNA) was utilized as a template, and RT-qPCR was performed on an iCycler Thermal Cycler with SYBR-Green supermix (Bio-Rad) and gene-specific oligonucleotide pairs (Supplementary Table S2). The PCR Base Line Subtracted Curve Fit mode was applied for threshold cycle (C_t), C_t values for target mRNAs were normalized to GAPDH mRNA, and the relative expression level of each target gene was calculated as already described.

Cardiac myocytes (1×10^6/well in six-well plate) were transfected with pBI.EGFP–MnSOD plasmid in triplicate (2 μg plasmid with 7 μl Lipofectamine 2000) as detailed in the plasmids and transient transfection section. Cells were infected with *T. cruzi* (1:5, cell:parasite ratio) for 24 h, washed, and suspended in TRIzol reagent (1 ml/well). Total RNA was isolated, and gene expression analysis was performed as already described.

Tissue homogenates and mitochondrial and nuclear fractions

Tissue sections (tissue:buffer ratio, 1:10 w/v) were homogenized in RIPA buffer (Cat. No. 9806; Cell Signaling, Dallas, TX), centrifuged at 10,000 *g*, and supernatants were used as tissue lysates. To isolate mitochondria, freshly harvested heart tissues were minced in ice-cold isolation buffer (10 m*M* HEPES pH 7.4, 225 m*M* mannitol, 75 m*M* sucrose, and 0.2% fatty acid-free bovine serum albumin [BSA]; tissue: HMSB ratio, 1:20), and homogenized in a dounce homogenizer in the presence of collagenase (200 U/ml). Collagenolysis was stopped with addition of 1 m*M* EGTA (ethylene glycol-bis(β-aminoethyl ether)-N,N,N′,N′-tetraacetic acid), and samples were centrifuged sequentially at 600 *g* and 8000 *g* to pellet the mitochondria (52). The nuclear fractions were prepared by employing Nuclear Complex Co-IP kit (Cat. No. 101690; Active Motif, Carlsbad, CA).

HeLa cells were cultured in six-well plates (1×10^6 cells per well) and transfected with pBI.EGFP–MnSOD (2 μg plasmid with 7 μl Lipofectamine 2000). Cells were harvested, suspended in HMSB medium (1.2×10^7 cells in 500 μl), and homogenized, and mitochondria were isolated by differential centrifugation as already described. Mitochondrial pellets were suspended in 100 μl HMSB medium and utilized to measure MnSOD expression by Western blotting.

Western blotting

Heart homogenates (30 μg protein) and isolated mitochondria (15 μg protein) or nuclear fractions (10 μg protein) were electrophoresed on a 4–15% Mini-Protein® TGX™ gel using a Mini-PROTEAN electrophoresis chamber (Bio-Rad), and proteins were transferred to a polyvinylidene fluoride membrane using a Criterion Trans-blot System (Bio-Rad). Membranes were blocked with 5% nonfat dry milk (NFDM) in 50 m*M* Tris-HCl (pH 7.5)/150 m*M* NaCl (TBS), washed with TBS–0.1% Tween 20 (TBST) and TBS, and incubated overnight at 4°C with antirabbit antibodies against NFE2L2 (Cat. No. 12721S, 1:1000; Cell Signaling), Keap1 (Cat. No. sc33569, 1:1000; Santa Cruz, Inc., Santa Cruz, CA), HO1 (Cat. No. 5061, 1:1000; Cell Signaling), MnSOD (Cat. No. PA1-31072, 1:5000; Life Technology, Carlsbad, CA), COX IV (Cat. No. ab16056, 1:2000; Abcam, San Francisco, CA), Lamin A/C (Cat. No. sc20681, 1:1000; Santa Cruz, Inc.), and GAPDH (Cat. No. 3683, 1:1000; Cell Signaling). All antibodies were diluted in TBST–2% NFDM. Membranes were washed as already described, incubated with horseradish peroxidase (HRP)-conjugated goat-antirabbit secondary antibody (Cat. No. 4041-05, 1:5000 dilution; Southern Biotech, Birmingham, AL), and signal captured by using an ImageQuant LAS4000 system (GE Healthcare, Pittsburgh, MA). Immunoblots were subjected to Ponceau S staining to confirm equal loading and transferring of samples. Densitometry analysis of protein bands was performed using a Fluorchem HD2 Imaging System (Alpha-Innotech, San Leandro, CA) and normalized against GAPDH (tissue homogenates), COX IV (mitochondrial fractions), or Lamin A/C (nuclear fractions).

In-tissue mitochondrial analysis and high-resolution respirometry

Freshly harvested LV tissues (~10 mg) were immersed in ice-cold BIOPS buffer (10 m*M* CaK_2–EGTA, 7.2 m*M* K_2–EGTA, 20 m*M* imidazole, 20 m*M* taurine, 50 m*M* K-MES, 0.5 m*M* dithiothreitol, 6.5 m*M* $MgCl_2$, 5.8 m*M* ATP, and 15 m*M* creatine phosphate; pH 7.1). Myofiber bundles were transferred to 2 ml of MIR05 buffer (0.5 m*M* EGTA, 3 m*M* $MgCl_2$, 60 m*M* K-lactobionate, 20 m*M* taurine, 10 m*M* KH_2PO_4, 20 m*M* HEPES, 110 m*M* sucrose, and 1 mg/ml fatty acid-free BSA, pH 7.1) containing 50 μg/ml saponin, and incubated at 4°C for 30 min to achieve chemical permeabilization of the sarcolemma membrane. Permeabilized myofiber bundles (~2 mg) were washed with MIR05 buffer and used for measuring mitochondrial respiration by using an O2K respirometer (Oroboros Instruments, Innsbruck, Austria). Oxygen concentration was determined at 2 s intervals and used to compute oxygen flux per milligram of tissue by Oroboros DatLab software (42). In brief, a leak respiratory state was recorded with myofiber bundles alone, and state 4 leak respiration supported by electron flow through CI (5 m*M* pyruvate, 10 m*M* glutamate, and 2 m*M* malate, P+G+M) was recorded. Electron transfer was coupled to phosphorylation by the addition of 5 m*M* ADP, and state 3 respiration supported by CI was recorded. Maximal state 3 respiration with parallel electron input from CI and CII was recorded with addition of 10 m*M* succinate, and CII-supported respiration was measured in the presence of 6.25 μM rotenone (inhibits CI). Cytochrome C (10 μM) was added to assess the

competence of the outer mitochondrial membrane. The absence of a significant increase in respiratory flux after the addition of cytochrome C indicates that the outer mitochondrial membranes are intact. Finally, maximal electron transfer capacity was recorded in the presence of 5 μM FCCP (42).

Respiration and ROS production in isolated cardiac mitochondria

A Mitocell S200A Respirometry System (Strathkelvin, Motherwell, United Kingdom) was used to measure the respiration rate in isolate mitochondria. In brief, a microcathode oxygen electrode was calibrated in 0.5 ml MSP buffer (225 mM mannitol, 75 mM sucrose, 20 mM KH_2PO_4/K_2HPO_4 pH 7.6). Freshly isolated cardiac mitochondria (200 μg) from WT and $MnSOD^{tg}$ (chronically infected and control) mice were suspended in 0.5 ml MSP buffer and added to the mitocell to record the basal O_2 consumption. The CI-supported state 4 respiration was recorded after adding P+G+M substrates. Then, 230 μM ADP was added and CI-driven state 3 respiration was recorded. Next, 5 mM succinate and 6.25 μM rotenone (S+R) were added to record the CII-supported state 3 respiration. Then, 5 μg/ml oligomycin was added and CII-driven state 4 was recorded. The ADP/O ratio (mitochondrial ATP production capacity) was calculated as decrease in O_2 concentration during state 3 respiration per O atom consumed (53).

To measure the rate of mtROS generation, cardiac mitochondria (25 μg protein) isolated from WT and $MnSOD^{tg}$ (chronically infected and control) mice were resuspended in 50 μl of HMS medium (10 mM HEPES pH 7.4, 225 mM mannitol, and 75 mM sucrose), and added in triplicate to 96-well, black flat-bottomed plate containing 50 μl of 2 × reaction buffer (20 mM Tris-HCl at pH 7.4, 500 mM sucrose, 2 mM EDTA) containing 66 μM Amplex Red and 0.2 U/ml HRP. Amplex Red oxidation by ROS to fluorescent resorufin was measured at Ex_{563nm}/Em_{587nm} on a SpectraMax M5 microplate reader (Molecular Devices, Sunnyvale, CA). After recording the baseline, P+G+M and ADP were added (as already described), and CI-driven ROS production was recorded for 5 min. Next, S + R were added, and CII-driven ROS production was recorded for 5 min. Standard curve was prepared with H_2O_2 (50 nM–5 μM) and data are presented as the rate of H_2O_2 production per minute per milligram mitochondrial protein. The percentage of mitochondrial electron leakage was calculated as the rate of $O_2^{\bullet -}$ production × 100/ 2 × rate of O_2 consumption (54).

Antioxidant and oxidant levels

TAC in plasma and isolated cardiac mitochondria of chronically infected WT and $MnSOD^{tg}$ mice (controls: matched, uninfected mice) were assessed by using lag time by antioxidants against the myoglobin-induced oxidation of 2,2′-azino-di(3-ethylbenzthiazoline-6-sulfonic acid) (ABTS) with H_2O_2. In brief, 20 μl of plasma samples (diluted 1:20, v/v) or isolated mitochondria (15 μg) was added in triplicate to 96-well plates and mixed with 90 μl of 10 mM phosphate-buffered saline (PBS; pH 7.2), 50 μl of myoglobin solution, and 20 μl of 3 mM ABTS. The reaction was initiated with H_2O_2 (20 μl) and change in color was monitored at 600 nm (standard curve: 2–25 μM trolox).

MnSOD activity in heart homogenates or isolated cardiac mitochondria was measured by using a Superoxide Dismutase Assay kit (Cat. No. 706002; Cayman Chemicals, Ann Arbor, MI). The assay utilizes a tetrazolium salt for detection of superoxide radicals generated in the presence of xanthine oxidase and hypoxanthine. One unit of SOD was defined as the amount of MnSOD needed to exhibit 50% dismutation of the superoxide radical (standard curve: 0.005–0.05 U/ml recombinant CuZnSOD).

Lipid peroxidation products in heart homogenates were measured by a TBARS assay. In brief, samples (1:10 w/v, 100 μl) were added in a glass tube containing 4 ml reaction mixture (0.4% sodium dodecyl sulfate [SDS], 7.5% acetic acid, pH 3.5, and 0.3% thiobarbituric acid), and heated at 95°C for 60 min. After cooling, samples were extracted with 5 ml n-butanol: pyridine (15:1, v/v), and absorbance was recorded at 532 nm ($\varepsilon = 1.56 \times 10^5\ M^{-1} \cdot cm^{-1}$).

The protein carbonyls in heart homogenates and isolated cardiac mitochondria of WT and $MnSOD^{tg}$ mice (normal and chronically infected) were measured by a colorimetric protein carbonyl assay (Cat. No. 10005020; Cayman Chemicals) according to the instructions provided by the manufacturer. Protein carbonyls in isolated cardiac mitochondria were also evaluated by Western blotting. In brief, carbonyls were derivatized with 2,4-dinitrophenylhydrazine for 30 min, and samples were neutralized and resolved by sodium dodecyl sulfate polyacrylamide gel electrophoresis (SDS-PAGE) as already described. DNP-derivatized, carbonyl proteins were detected by using an anti-DNP antibody (Cat. No. D9656, antirabbit IgG, 1:5000; Sigma, St. Louis, MO).

The H_2O_2 levels in heart homogenates were measured by Amplex Red assay. In brief, 50 μl of tissue lysates (100 μg protein) was pipetted into a black 96-well plate, and 100 μl of reaction mixture containing 0.05 M sodium phosphate, pH 7.4, 33 μM Amplex Red, and 0.1 U/ml HRP was added. The plate was read at Ex_{563nm}/Em_{587nm} after incubating for 30 min in the dark and calculated as already described.

To measure H_2O_2 in cells, HeLa cells (1×10^4/well) were transfected with pBI.EGFP–MnSOD and infected with *T. cruzi* for 24 h. Cells were washed twice with PBS, suspended in color-free RPMI, and H_2O_2 levels were measured by Amplex Red assay as already described.

Mitochondrial membrane potential

Mitochondrial membrane potential in HeLa cells was assessed with TMRE (Cat. No. T669; Molecular Probes, Eugene, OR). In brief, HeLa cells were transfected with pBI.EGFP–MnSOD, seeded in the 96-well plate, and infected with *T. cruzi* for 1 h. Cells were washed to remove free parasites and loaded with TMRE (100 nM) at 37°C for 30 min. Cells were incubated for 0, 3, 6, 12, and 24 h, and mean fluorescence intensity was measured at Ex_{549nm}/Em_{574nm}.

NFE2L2-double-stranded DNA binding assay

The nuclear fractions (5 μg) from the heart tissue of WT and $MnSOD^{tg}$ mice (normal and *Tc* infected) were added in triplicate to the 96-well plate precoated with double-stranded DNA (dsDNA) sequence containing the NFE2L2 response element (Cat. No. 600590; Cayman Chemicals). Plates were incubated overnight at room temperature, washed five times with wash buffer to remove unbound proteins, and then sequentially incubated at room temperature for 1 h each with anti-NFE2L2 primary antibody and goat antirabbit HRP-

conjugated secondary antibody. The signal was developed using 3,3′,5,5′-tetramethylbenzidine substrate and change in absorbance was measured at 450 nm.

NFE2L2 transcriptional activity

HeLa cells (10^4/well) were seeded in 96-well tissue-culture plates, and incubated overnight in antibiotic-free Opti-MEM. Cells were transfected with pRL-SV40 plasmid (50 ng) in combination with pBI.EGFP–MnSOD and/or luciferase reporter plasmids (100 ng each) using Lipofectamine 2000 reagent (Invitrogen). After 6 h of incubation, cells were washed, replenished with complete medium for 3–5 h, and then infected with *T. cruzi* (cell:parasite ratio, 1:5). The relative NFE2L2 transcriptional activity for HO1, GCLM, and NQO1 was measured by using a Dual Luciferase Assay System (Promega) and normalized to Renilla luciferase activity.

Confocal microscopy

Cultured cardiac myocytes were seeded (10^4 cells/well) in Lab-Tek II eight-well chamber slides (Nunc, Rochester, NY) and incubated overnight at 37°C, 5% CO_2. Cells were transfected with pBI.EGFP–MnSOD and infected with *T. cruzi* for 24 h as already described. Cells were washed three times with PBS and fixed/permeabilized using ice-cold acetone/methanol (1:1, v/v). Cells were blocked for 1 h with 1% BSA/0.2% gelatin in PBS–0.2% Triton X-100, and incubated overnight at 4°C with anti-NFE2L2 antibody (1:200 dilution) and then for 1 h at room temperature with Alexa Fluor 568 conjugated secondary antibody (Cat. No. A10042; Molecular Probes). Cells were counter stained with DAPI (blue fluorescence, nuclear). The NFE2L2 (Ex_{578nm}/Em_{603nm}) and DAPI (Ex_{340nm}/Em_{488nm}) fluorescence were observed using a Zeiss LSM 510 confocal microscope (Leica Microsystems, Wetzlar, Germany) with a 100× oil immersion lens, and images were collected using a C-Mount 1500M-GE camera at the UTMB Optical Microscopy Core Facility.

ECG assessment of LV structure and function

Mice were continuously anesthetized by inhalant 1.5% isoflurane/100% O_2 to maintain a light sedation level. Mice were placed supine on an electrical heating pad at 37°C during the examination. The ECG electrodes of the Vevo 2100 ultrasound system (Visual Sonics, Toronto, Canada) were connected to mouse paws, and heart rate and respiratory physiology were continuously monitored. Mice chests were shaved, and warmed ultrasound gel was applied to the area of interest. Transthoracic ECG was performed using the high-frequency linear array transducer (MS400, 18–38 MHz) of the Vevo 2100 ultrasound system (7). Heart was imaged in B-mode and M-mode to examine the parameters of LV in diastole (-d) and systole (-s). Pulse wave Doppler imaging was performed to measure heart diastolic function, including early (E) to late ventricular filling velocity (E/A ratio), IVRT, IVCT, LVET, and MPI = [IVCT + IVRT]/LVET. All measurements were obtained in triplicate and data were analyzed by using Vevo 2100 standard measurement software.

Histology

Tissue sections were fixed in 10% buffered formalin, dehydrated in absolute ethanol, cleared in xylene, and embedded in paraffin. Five-micron tissue sections were subjected to Masson's Trichrome staining at the Research Histopathology Core at the UTMB, and fibrosis was assessed by measuring the collagen area as a percentage of the total myocardial area ($n = 4$/group, 10 regions per heart) using simple PCI software (v.6.0; Compix, Sewickley, PA). Sections were categorized based on percentage fibrotic area: (0) <1%, (1) 1–5%, (2) 5–10%, (3) 10–15%, and (4) >15% (13).

Data analysis

All experiments were conducted with triplicate observations per sample ($n = 6$–10 mice/group), and data are expressed as mean ± standard error of the mean (SEM). All data were analyzed using GraphPad Prism 5 (GraphPad Software, La Jolla, CA). Data (linear range or $\log_{10}$ transformed) were analyzed by the Kolmogorov–Smirnov test to determine whether the data are normally distributed. When data were normally distributed, Student's *t* test (comparison of two groups) and one-way analysis of variance (ANOVA) with Tukey's test (comparison of multiple groups) were applied. If data were not normally distributed, then Mann–Whitney test (comparison of two groups) and Kruskal–Wallis with Dunn's test (comparison of multiple groups) were employed. Significance is presented by *(infected *vs.* matched control) and $^{\#}$(MnSOD^{tg} *vs.* WT or MnSOD^{tg}.*Tc vs.* WT.*Tc*) ($^{*,\#}p < 0.05$, $^{**,\#\#}p < 0.01$, $^{***,\#\#\#}p < 0.001$).

Acknowledgments

This work was supported, in part, by grants from the National Institute of Allergy and Infectious Diseases (2R01AI054578) and National Heart Lung Blood Institute (R01HL094802) of the National Institutes of Health to N.J.G. A minicenter pilot grant from the Institute for Human Infections and Immunity, UTMB (Galveston, TX), also supported part of the presented studies.

Authors' Contributions

N.J.G. provided financial support, conceived the study, and wrote the article. J.J.W. performed the experiments, analyzed the data, and helped in article writing. C.P. participated in metabolic studies.

Author Disclosure Statement

No competing financial interests exist.

References

1. Acquatella H. Echocardiography in Chagas heart disease. *Circulation* 115: 1124–1131, 2007.
2. Acquatella H, Schiller NB, Puigbo JJ, Giordano H, Suarez JA, Casal H, *et al.* M-mode and two-dimensional echocardiography in chronic Chages' heart disease. A clinical and pathologic study. *Circulation* 62: 787–799, 1980.
3. Ahmed KM and Li JJ. NF-kappa B-mediated adaptive resistance to ionizing radiation. *Free Radic Biol Med* 44: 1–13, 2008.
4. Ba X, Gupta S, Davidson M, and Garg NJ. *Trypanosoma cruzi* induces the reactive oxygen species-PARP-1-RelA pathway for up-regulation of cytokine expression in cardiomyocytes. *J Biol Chem* 285: 11596–11606, 2010.

5. Baldelli S, Aquilano K, and Ciriolo MR. Punctum on two different transcription factors regulated by PGC-1alpha: Nuclear factor erythroid-derived 2-like 2 and nuclear respiratory factor 2. *Biochim Biophys Acta* 1830: 4137–4146, 2013.
6. Barros MV, da Costa Rocha MO, Ribeiro AL, and Machado FS. Tissue Doppler imaging enables the identification of diastolic dysfunction of pseudonormal pattern in Chagas' disease. *J Am Soc Echocardiogr* 14: 353–359, 2001.
7. Bhan A, Sirker A, Zhang J, Protti A, Catibog N, Driver W, *et al.* High-frequency speckle tracking echocardiography in the assessment of left ventricular function and remodeling after murine myocardial infarction. *Am J Physiol Heart Circ Physiol* 306: H1371–H1383, 2014.
8. Biering-Sorensen T, Mogelvang R, Schnohr P, and Jensen JS. Cardiac time intervals measured by tissue Doppler imaging M-mode: Association with hypertension, left ventricular geometry, and future ischemic cardiovascular diseases. *J Am Heart Assoc* 5, pii: e002687, 2016.
9. Botoni FA, Poole-Wilson PA, Ribeiro AL, Okonko DO, Oliveira BM, Pinto AS, *et al.* A randomized trial of carvedilol after renin-angiotensin system inhibition in chronic Chagas cardiomyopathy. *Am Heart J* 153: 544.e541–e548, 2007.
10. Budni P, Pedrosa RC, Dalmarco EM, Dalmarco JB, Frode TS, and Wilhelm Filho D. Carvedilol enhances the antioxidant effect of vitamins E and C in chronic Chagas heart disease. *Arq Bras Cardiol* 101: 304–310, 2013.
11. Candas D and Li JJ. MnSOD in oxidative stress response-potential regulation via mitochondrial protein influx. *Antioxid Redox Signal* 20: 1599–1617, 2014.
12. Cunha-Neto E, Dzau VJ, Allen PD, Stamatiou D, Benvenutti L, Higuchi ML, *et al.* Cardiac gene expression profiling provides evidence for cytokinopathy as a molecular mechanism in Chagas' disease cardiomyopathy. *Am J Pathol* 167: 305–313, 2005.
13. Dhiman M and Garg NJ. NADPH oxidase inhibition ameliorates *Trypanosoma cruzi*-induced myocarditis during Chagas disease. *J Pathol* 225: 583–596, 2011.
14. Dhiman M, Wan X, Popov VL, Vargas G, and Garg NJ. $MnSOD^{tg}$ mice control myocardial inflammatory and oxidative stress and remodeling responses elicited in chronic Chagas disease. *J Am Heart Assoc* 2: e000302, 2013.
15. Ding G, Fu M, Qin Q, Lewis W, Kim HW, Fukai T, *et al.* Cardiac peroxisome proliferator-activated receptor gamma is essential in protecting cardiomyocytes from oxidative damage. *Cardiovasc Res* 76: 269–279, 2007.
16. Erkens R, Kramer CM, Luckstadt W, Panknin C, Krause L, Weidenbach M, *et al.* Left ventricular diastolic dysfunction in Nrf2 knock out mice is associated with cardiac hypertrophy, decreased expression of SERCA2a, and preserved endothelial function. *Free Radic Biol Med* 89: 906–917, 2015.
17. Fan D, Takawale A, Lee J, and Kassiri Z. Cardiac fibroblasts, fibrosis and extracellular matrix remodeling in heart disease. *Fibrogenesis Tissue Repair* 5: 15, 2012.
18. Feuerstein G, Yue TL, Ma X, and Ruffolo RR. Novel mechanisms in the treatment of heart failure: Inhibition of oxygen radicals and apoptosis by carvedilol. *Prog Cardiovasc Dis* 41: 17–24, 1998.
19. Galderisi M. Diastolic dysfunction and diastolic heart failure: diagnostic, prognostic and therapeutic aspects. *Cardiovasc Ultrasound* 3: 9, 2005.
20. Garg N, Popov VL, and Papaconstantinou J. Profiling gene transcription reveals a deficiency of mitochondrial oxidative phosphorylation in *Trypanosoma cruzi*-infected murine hearts: Implications in chagasic myocarditis development. *Biochim Biophys Acta* 1638: 106–120, 2003.
21. Garzoni LR, Adesse D, Soares MJ, Rossi MI, Borojevic R, and de Meirelles Mde N. Fibrosis and hypertrophy induced by *Trypanosoma cruzi* in a three-dimensional cardiomyocyte-culture system. *J Infect Dis* 197: 906–915, 2008.
22. Gupta S and Garg NJ. A Two-component DNA-prime/protein-boost vaccination strategy for eliciting long-term, protective T cell immunity against *Trypanosoma cruzi*. *PLoS Pathog* 11: e1004828, 2015.
23. Gupta S, Wen JJ, and Garg NJ. Oxidative stress in Chagas disease. *Interdiscip Perspect Infect Dis* 2009: 190354, 2009.
24. Hegstad AC, Ytrehus K, Myklebust R, and Jorgensen L. Ultrastructural changes in the myocardial myocytic mitochondria: Crucial step in the development of oxygen radical-induced damage in isolated rat hearts? *Basic Res Cardiol* 89: 128–138, 1994.
25. Higuchi MD, Benvenuti LA, Martins Reis M, and Metzger M. Pathophysiology of the heart in Chagas' disease: Current status and new developments. *Cardiovasc Res* 60: 96–107, 2003.
26. Hovsepian E, Penas F, Mirkin GA, and Goren NB. Role of PPARs in *Trypanosoma cruzi* infection: Implications for Chagas disease therapy. *PPAR Res* 2012: 528435, 2012.
27. Huang H, Petkova SB, Cohen AW, Bouzahzah B, Chan J, Zhou JN, *et al.* Activation of transcription factors AP-1 and NF-kappa B in murine Chagasic myocarditis. *Infect Immun* 71: 2859–2867, 2003.
28. Hurttila H, Koponen JK, Kansanen E, Jyrkkanen HK, Kivela A, Kylatie R, *et al.* Oxidative stress-inducible lentiviral vectors for gene therapy. *Gene Ther* 15: 1271–1279, 2008.
29. Itoh K, Ye P, Matsumiya T, Tanji K, and Ozaki T. Emerging functional cross-talk between the Keap1-Nrf2 system and mitochondria. *J Clin Biochem Nutr* 56: 91–97, 2015.
30. Jang YC, Perez VI, Song W, Lustgarten MS, Salmon AB, Mele J, *et al.* Overexpression of Mn superoxide dismutase does not increase life span in mice. *J Gerontol A Biol Sci Med Sci* 64: 1114–1125, 2009.
31. Kops GJ, Dansen TB, Polderman PE, Saarloos I, Wirtz KW, Coffer PJ, *et al.* Forkhead transcription factor FOXO3a protects quiescent cells from oxidative stress. *Nature* 419: 316–321, 2002.
32. Koshy SK, Reddy HK, and Shukla HH. Collagen cross-linking: new dimension to cardiac remodeling. *Cardiovasc Res* 57: 594–598, 2003.
33. Lai L, Yan L, Gao S, Hu CL, Ge H, Davidow A, *et al.* Type 5 adenylyl cyclase increases oxidative stress by transcriptional regulation of manganese superoxide dismutase via the SIRT1/FoxO3a pathway. *Circulation* 127: 1692–1701, 2013.
34. Lustgarten MS, Jang YC, Liu Y, Qi W, Qin Y, Dahia PL, *et al.* MnSOD deficiency results in elevated oxidative stress and decreased mitochondrial function but does not lead to muscle atrophy during aging. *Aging Cell* 10: 493–505, 2011.
35. Machado FS, Dutra WO, Esper L, Gollob KJ, Teixeira MM, Weiss LM, *et al.* Current understanding of immunity to *Trypanosoma cruzi* infection and pathogenesis of Chagas disease. *Semin Immunopathol* 34: 753–770, 2012.
36. Maehara K, Uekawa N, and Isobe K. Effects of histone acetylation on transcriptional regulation of manganese superoxide dismutase gene. *Biochem Biophys Res Commun* 295: 187–192, 2002.

37. Migliore RA, Adaniya ME, Tamagusuku H, and Lapuente A. Assessment of diastolic function in Chagas' disease with pulsed Doppler tissue imaging. *Arch Cardiol Mex* 74: 31–38, 2004.
38. Nakamura TY, Yamamoto I, Kanno Y, Shiba Y, and Goshima K. Metabolic coupling of glutathione between mouse and quail cardiac myocytes and its protective role against oxidative stress. *Circ Res* 74: 806–816, 1994.
39. Nguyen T, Nioi P, and Pickett CB. The Nrf2-antioxidant response element signaling pathway and its activation by oxidative stress. *J Biol Chem* 284: 13291–13295, 2009.
40. Nowotny K, Jung T, Hohn A, Weber D, and Grune T. Advanced glycation end products and oxidative stress in type 2 diabetes mellitus. *Biomolecules* 5: 194–222, 2015.
41. Nunes Mdo C, Barbosa MM, and Rocha MO. Peculiar aspects of cardiogenic embolism in patients with Chagas' cardiomyopathy: A transthoracic and transesophageal echocardiographic study. *J Am Soc Echocardiogr* 18: 761–767, 2005.
42. Porter C, Herndon DN, Bhattarai N, Ogunbileje JO, Szczesny B, Szabo C, *et al.* Differential acute and chronic effects of burn trauma on murine skeletal muscle bioenergetics. *Burns* 42: 112–122, 2016.
43. Raineri I, Carlson EJ, Gacayan R, Carra S, Oberley TD, Huang TT, *et al.* Strain-dependent high-level expression of a transgene for manganese superoxide dismutase is associated with growth retardation and decreased fertility. *Free Radic Biol Med* 31: 1018–1030, 2001.
44. Sen T, Sen N, Noordhuis MG, Ravi R, Wu TC, Ha PK, *et al.* OGDHL is a modifier of AKT-dependent signaling and NF-kappaB function. *PLoS One* 7: e48770, 2012.
45. Tanowitz HB, Machado FS, Spray DC, Friedman JM, Weiss OS, Lora JN, *et al.* Developments in the management of Chagas cardiomyopathy. *Expert Rev Cardiovasc Ther* 13: 1393–1409, 2015.
46. Tanowitz HB, Weiss LM, and Montgomery SP. Chagas disease has now gone global. *PLoS Negl Trop Dis* 5: e1136, 2011.
47. Tanowitz HB, Wen JJ, Machado FS, Desruisseaux MS, Robello C, and Garg NJ. *Trypanosoma cruzi* and Chagas disease: innate immunity, ROS, and cardiovascular system. In: *Vascular Responses to Pathogens*, edited by Gavins FNE and Stokes KY. Waltham, MA: Academic Press/Elsevier, Inc., 2016, pp. 183–195.
48. Tao R, Vassilopoulos A, Parisiadou L, Yan Y, and Gius D. Regulation of MnSOD enzymatic activity by Sirt3 connects the mitochondrial acetylome signaling networks to aging and carcinogenesis. *Antioxid Redox Signal* 20: 1646–1654, 2014.
49. Tufekci KU, Civi Bayin E, Genc S, and Genc K. The Nrf2/ARE pathway: A promising target to counteract mitochondrial dysfunction in Parkinson's disease. *Parkinsons Dis* 2011: 314082, 2011.
50. Udoko AN, Johnson CA, Dykan A, Rachakonda G, Villalta F, Mandape SN, *et al.* Early regulation of profibrotic genes in primary human cardiac myocytes by *Trypanosoma cruzi*. *PLoS Negl Trop Dis* 10: e0003747, 2016.
51. Wan X, Gupta S, Zago MP, Davidson MM, Dousset P, Amoroso A, *et al.* Defects of mtDNA replication impaired mitochondrial biogenesis during *Trypanosoma cruzi* infection in human cardiomyocytes and chagasic patients: The role of Nrf1/2 and antioxidant response. *J Am Heart Assoc* 1: e003855, 2012.
52. Wen JJ, Dhiman M, Whorton EB, and Garg NJ. Tissue-specific oxidative imbalance and mitochondrial dysfunction during *Trypanosoma cruzi* infection in mice. *Microbes Infect* 10: 1201–1209, 2008.
53. Wen JJ and Garg NJ. Mitochondrial complex III defects contribute to inefficient respiration and ATP synthesis in the myocardium of *Trypanosoma cruzi*-infected mice. *Antioxid Redox Signal* 12: 27–37, 2010.
54. Wen JJ and Garg NJ. Mitochondrial generation of reactive oxygen species is enhanced at the Q(o) site of the complex III in the myocardium of *Trypanosoma cruzi*-infected mice: beneficial effects of an antioxidant. *J Bioenerg Biomembr* 40: 587–598, 2008.
55. Wen JJ, Gupta S, Guan Z, Dhiman M, Condon D, Lui C, *et al.* Phenyl-alpha-tert-butyl-nitrone and benzonidazole treatment controlled the mitochondrial oxidative stress and evolution of cardiomyopathy in chronic chagasic rats. *J Am Coll Cardiol* 55: 2499–2508, 2010.
56. Wen JJ, Vyatkina G, and Garg N. Oxidative damage during chagasic cardiomyopathy development: Role of mitochondrial oxidant release and inefficient antioxidant defense. *Free Radic Biol Med* 37: 1821–1833, 2004.
57. Wen JJ, Yachelini PC, Sembaj A, Manzur RE, and Garg NJ. Increased oxidative stress is correlated with mitochondrial dysfunction in chagasic patients. *Free Radic Biol Med* 41: 270–276, 2006.
58. Yen HC, Oberley TD, Vichitbandha S, Ho YS, St and Clair DK. The protective role of manganese superoxide dismutase against adriamycin-induced acute cardiac toxicity in transgenic mice. *J Clin Invest* 98: 1253–1260, 1996.
59. Zacks MA, Wen JJ, Vyatkina G, Bhatia V, and Garg NJ. An overview of chagasic cardiomyopathy: pathogenic importance of oxidative stress. *An Acad Bras Cienc* 77: 695–715, 2005.

Address correspondence to:
Dr. Nisha Jain Garg
Department of Microbiology and Immunology
University of Texas Medical Branch (UTMB)
3.142C Medical Research Building
301, University Boulevard
Galveston TX 77555-1070

E-mail: nigarg@utmb.edu

Date of first submission to ARS Central, July 14, 2016; date of final revised submission, January 25, 2017; date of acceptance, January 26, 2017.

Abbreviations Used

ABTS = 2,2′-azino-di(3-ethylbenzthiazoline-6-sulfonic acid
ARE = antioxidant response element
BSA = bovine serum albumin
CCM = chagasic cardiomyopathy
CI = complex I
CII = complex II
CO = cardiac output
C_t = threshold cycle
DMEM = Dulbecco's modified Eagle's medium
ECG = echocardiography
EF = ejection fraction
ESV = end systolic volume

Abbreviations Used (Cont.)

FBS = fetal bovine serum
FCCP = carbonyl cyanide-4-(trifluoromethoxy) phenyl-hydrazone
γGCS = gamma-glutamyl cysteine synthase
GCLM = glutamate-cysteine ligase modifier subunit
GST = glutathione S transferase
H_2O_2 = hydrogen peroxide
HO1 = heme oxygenase-1
HRP = horseradish peroxidase
IVCT = isovolumic contraction time
IVRT = isovolumetric relaxation time
IVS = interventricular septum
Keap1 = Kelch-like ECH-associated protein 1
LV = left ventricle
LVID = LV internal diameter
LVPW = LV posterior wall
MDA = malondialdehyde
MnSOD = manganese superoxide dismutase (mitochondrial)
mRNA = messenger RNA
mtROS = mitochondrial reactive oxygen species
MVET = mitral valve ejection time
NFDM = nonfat dry milk
NFE2L2 = nuclear factor (erythroid 2)-like 2
NQO1 = NAD(P)H dehydrogenase, quinone 1;
O2K = Oxygraph-2k
OXPHOS = oxidative phosphorylation
PBS = phosphate-buffered saline
PCR = polymerase chain reaction
P+G+M = pyruvate+glutamate+malate
pi = postinfection
PPAR = peroxisome proliferator-activated receptor
RCR = respiratory control ratio
SDS = sodium dodecyl sulfate
SDS-PAGE = sodium dodecyl sulfate polyacrylamide gel electrophoresis
S+R = succinate+rotenone
SV = stroke volume
Tc or *T. cruzi* = *Trypanosoma cruzi*
TMRE = tetramethylrhodamine, ethyl ester
Trx = thioredoxin
WT = wild type